Neutron-Capture Elements in the Early Galaxy

Christopher Sneden,[1] John J. Cowan,[2] and Roberto Gallino[3]

[1]Department of Astronomy, The University of Texas, Austin, Texas 78712; email: chris@verdi.as.utexas.edu

[2]Homer L. Dodge Department of Physics and Astronomy, University of Oklahoma, Norman, Oklahoma 73019; email: cowan@nhn.ou.edu

[3]Dipartimento di Fisica Generale, Università di Torino, 10125 Torino, Italy, and Center for Stellar and Planetary Astrophysics, School of Mathematical Sciences, Monash University, Victoria 3800, Australia; email: gallino@ph.unito.it

Annu. Rev. Astron. Astrophys. 2008. 46:241–88

First published online as a Review in Advance on June 27, 2008

The *Annual Review of Astronomy and Astrophysics* is online at astro.annualreviews.org

This article's doi: 10.1146/annurev.astro.46.060407.145207

0066-4146/08/0922-0241$20.00

Key Words

abundances, Galaxy evolution, nuclear reactions, nucleosynthesis, Population II, stars

Abstract

The content of neutron-capture (trans-iron-peak) elements in the low-metallicity Galactic halo varies widely from star to star. The differences are both in bulk amount of the neutron-capture elements with respect to lighter ones and in element-to-element ratios among themselves. Several well-defined abundance distributions have emerged that reveal characteristic rapid and slow neutron-capture nucleosynthesis patterns. In this review we summarize these observed metal-poor star's abundances, contrasting them with the Solar-system values, comparing them to theoretical predictions, using them to assess the types of stars responsible for their specific anomalies, and speculating on the timing and nature of early Galactic nucleosynthesis.

1. INTRODUCTION

Creation of the elements of the Periodic Table through stellar nucleosynthesis has been a vital astrophysical research area for nearly a century. Beginning with the Payne (1925) and Russell (1929) studies of the spectra of the Sun and nearby stars, efforts to understand element genesis remain near the top of modern physics interests (Turner et al. 2003). Each element isotope is synthesized in unique ways, but we recognize several element groups with similar dominant formation mechanisms. Shorthand names are given to these groups, whose memberships can be overlapping. The light elements with even atomic numbers whose major isotopes are multiples of ^{4}He nuclei are called the α elements. Those accessible to visible-infrared high-resolution spectroscopy include C, O, Mg, Si, S, and Ca (usually joined unofficially by Ti, whose major isotope is ^{48}Ti). Light elements whose abundances can be altered by hydrogen fusion reactions during quiescent stellar evolution (formally all those with $Z \leq 13$) are called proton-capture. Common usage includes observable C, N, O, F, Na, Mg, and Al in this group. The "Fe-peak" elements are those with $21 \leq Z \leq 30$, with the possible exception of Ti and Cu.

Elements with $Z > 30$ are labeled neutron-capture (*n*-capture). There are 54 stable or long-lived (half-life $\tau_{1/2} > 10^6$ years) *n*-capture elements, compared to only 30 lighter elements. Their aggregate content is very small, only $\sim 10^{-6}$% by number of Solar material. In spite of their tiny abundances, *n*-capture elements can produce significant spectral line absorption, and thus are detectable in stars over a wide metallicity range. Today we know detailed *n*-capture abundance distributions in many extremely metal-poor Galactic field stars, and have information on these elements in globular clusters and extragalactic systems. This information yields new insight on *n*-capture production in early Galactic epochs, which in turn probes the nature of earliest nucleosynthesis and helps identify the so-called first stars in the Galaxy.

Discovery of ultralow-metallicity halo stars has figured prominently in surveys of the Galactic halo. Three prominent examples have turned up: HE 0107-5240 ([Fe/H] ~ -5.3, Christlieb et al. 2002); HE 1327-2326 ([Fe/H] ~ -5.5, Frebel et al. 2005); and HE 0557-4840 ([Fe/H] ~ -4.8, Norris et al. 2007). All of these stars are extremely carbon-rich, [C/Fe] $> +1.5$. Sr is overabundant in HE 1327-2326, [Sr/Fe] $\sim +1$. Production of Sr for this star may have occurred via supernova nucleosynthesis and/or the *r*-process rather than with the *s*-process. However, because no other *n*-capture elements have been detected in these three stars, and the published upper limits do not provide useful information on the *r*-process and *s*-process, we do not consider ultralow-metallicity stars further here.

Other aspects of Galactic halo populations, structure, evolution, and nucleosynthesis have been discussed in recent *ARA&A* reviews: VandenBerg, Bolte & Stetson (1996: globular cluster ages); McWilliam (1997: abundances and chemical evolution); Wallerstein & Knapp (1998: carbon-rich stars); Freeman & Bland-Hawthorn (2002: stellar populations); Bromm & Larson (2004: early galaxy and star formation); Gratton, Sneden & Carretta (2004: globular cluster abundances); and Beers & Christlieb (2005: Galactic halo surveys).

In Section 2 we review the basic mechanisms of *n*-capture element synthesis, following in Section 3 with a discussion of Solar photospheric and Solar-system meteoritic abundances. Summaries of *n*-capture abundance results in low-metallicity stars enhanced in *r*-process and *s*-process elements appear in Section 4 and Section 5, respectively. Comparison of *r*-process theory and observation is carried out in Section 6, and in Section 7 we discuss implications for early nucleosynthesis and the age of our Galaxy. Interpretation of *s*-process-rich stars is developed in Section 8. Section 9 lists our conclusions.

2. HEAVY ELEMENT FORMATION

Stellar fusion of elements heavier than iron is endothermic: It requires energy. Also, Coulomb barriers for charged-particle reactions increase at heavy proton number. As a result, the nuclei beyond the Fe group are generally not formed in charged-particle fusion but instead are created in *n*-capture processes; there are no Coulomb barriers. Neutrons are captured onto nuclei that can then β decay if they are unstable, transforming neutrons into protons. In this manner, element production progresses through the heaviest elements of the Periodic Table. This process is defined as slow (rapid) if the timescale for neutron capture, τ_n, is slower (faster) than the radioactive decay timescale, for unstable nuclei. Generally we refer to these as the *s*-process or the *r*-process.

The *r*-process and *s*-process were initially described and defined in 1957 by Burbidge et al. (1957) and Cameron (1957a,b). The *s*-process ($\tau_n \gg \tau_\beta$) is defined by virtue of the long times (hundreds or thousands of years) between successive neutron captures on target nuclei. It thus operates close to the so-called valley of β-stability, as illustrated in **Figure 1** (Möller, Nix & Kratz 1997, their figure 16). Consequently the properties (e.g., masses and half-lives) of the stable and long-lived nuclei involved in the *s*-process can be obtained experimentally. As the *s*-process

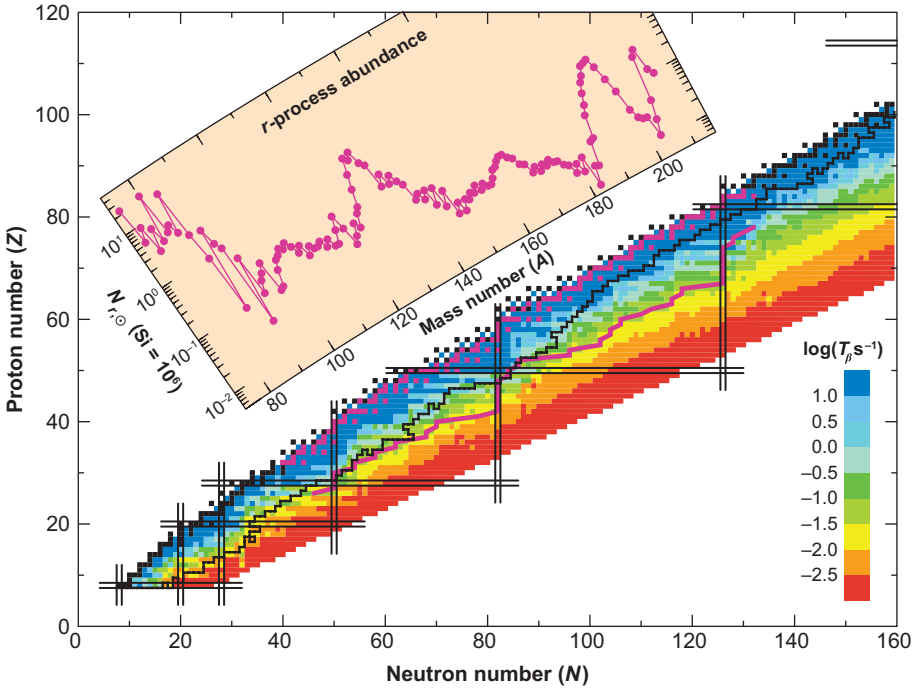

Figure 1

Chart of the nuclides showing proton number versus neutron number after Möller, Nix & Kratz (1997). Black boxes indicate stable nuclei and define the so-called valley of β-stability. Vertical and horizontal lines indicate closed proton or neutron shells. The magenta line indicates the so called *r*-process path, with the magenta boxes indicating where there are final stable *r*-process isotopes. Color shading denotes the timescales for β decay for nuclei and the jagged black line denotes the limits of experimentally determined nuclear data at the time of their article.

progresses, an unstable nuclide at the end of the isotope chain of an element with charge Z normally will suffer a β^- decay instead of capturing a further neutron, jumping from that unstable isotope to the isobar of the next element of charge Z + 1.

The details of the *r*-process are quite different from the *s*-process (see the following *r*-process reviews: Hillebrandt 1978; Mathews & Cowan 1990; Cowan, Thielemann & Truran 1991a; Meyer 1994; Truran et al. 2002; Sneden & Cowan 2003; Cowan & Thielemann 2004; and Arnould, Goriely & Takahashi 2008). Here large numbers of neutrons are captured per second with $\tau_n \ll \tau_\beta$. As a result, element synthesis occurs far from stability in neutron-rich (and very radioactive) regions (see **Figure 1**). The abundance distribution is produced as a result of the competition between photodisintegration and neutron captures, operating in chemical equilibrium, in each isotopic chain. The so-called *r*-process path (the *magenta line* in **Figure 1**) is then defined by the maximum abundance in all isotopic chains. After capturing a large number of neutrons these synthesized (unstable) nuclei in the path will eventually decay back to stability and form stable *r*-process nuclei (*magenta boxes* in **Figure 1**). Owing to the short radioactive half-lives (typically 0.01–0.1 seconds) of the isotopes involved in this process, experimental determinations of the properties (e.g., masses) of most of the *r*-process nuclei are generally not (yet) possible, although there have been some experimental advancements (see, e.g., Dillmann et al. 2003). For this reason we must rely on theoretical prescriptions, and particularly on formulas to predict nuclear masses, for many of the properties of the very neutron-rich nuclei that participate in the *r*-process (e.g., Lunney, Pearson & Thibault 2003). See Cowan & Thielemann (2004) for more *r*-process discussion.

We illustrate these synthesis processes in **Figure 2** by concentrating on elements Xe to Pr. The stable and long-lived isotopes that contribute more than 1% of their Solar-system elemental abundances are in the mass range $128 \leq A \leq 142$. The zig-zag turquoise-colored line traces the *s*-process path, which we extend in **Figure 2** through ^{142}Nd both to show the path direction immediately after ^{141}Pr and to emphasize the isotopic buildup at the N = 82 magic number. The diagonal green lines going from lower-right to upper-left indicate the β-decay direction of neutron-rich (radioactive) nuclei in the *r*-process path.

About 35 heavy nuclides from ^{96}Mo to ^{204}Pb are called *s*-only nuclei, because they are shielded (i.e., blocked from below) against the *r*-process by the corresponding stable isobar of charge Z – 2. This is the case of the pair ^{134,136}Ba, shielded against the *r*-process by ^{134,136}Xe, respectively. Long-lived isotopes like ^{93}Zr, ^{99}Tc, or ^{107}Pd that are encountered along the *s*-path mostly behave as stable nuclides during the neutron fluence and will afterward provide a consistent *s*-process-radiogenic abundance to ^{93}Nb, ^{99}Ru, or ^{107}Ag.

Isotopes dominated by the *s*-process form close to β-stability; for these nuclides experimental measurements are possible. There are several approaches to obtaining *s*-process abundances N_s, utilizing experimental capture cross sections $\sigma_{n,\gamma}$ (hereafter simply σ). The "classical" model assumes a smoothly varying behavior of the σN_s product for nuclides lying along the *s*-process path away from neutron magic nuclei N = 50, 82, and 126. The σN_s curve has steep decreases at the magic neutron numbers, for which σ values are very small and thus N_s yields are large. These yield the first *s*-process-peak at Sr, Y, Zr (light-*s* elements, hereafter called "ls") and the second peak at Ba, La, Ce, Pr, Nd (heavy-*s*, or "hs") and eventually the third peak at the termination point of the *s*-process, Pb and Bi.

From analysis of the Solar σN_s curve, without considering stellar nucleosynthesis sources for the *s*-process, Clayton et al. (1961) and Seeger, Fowler & Clayton (1965) derived basic properties of the *s*-process (a good summary is Clayton 1968, chapter 7). They concluded that the *s*-process is a dynamical one, consisting of at least three clearly defined parts. The "main" component, accounting for the bulk of the *s*-process distribution in the Solar-system for nuclei with $88 \leq A \leq 204$, can be reproduced by a continuous distribution of decreasing neutron exposures. An

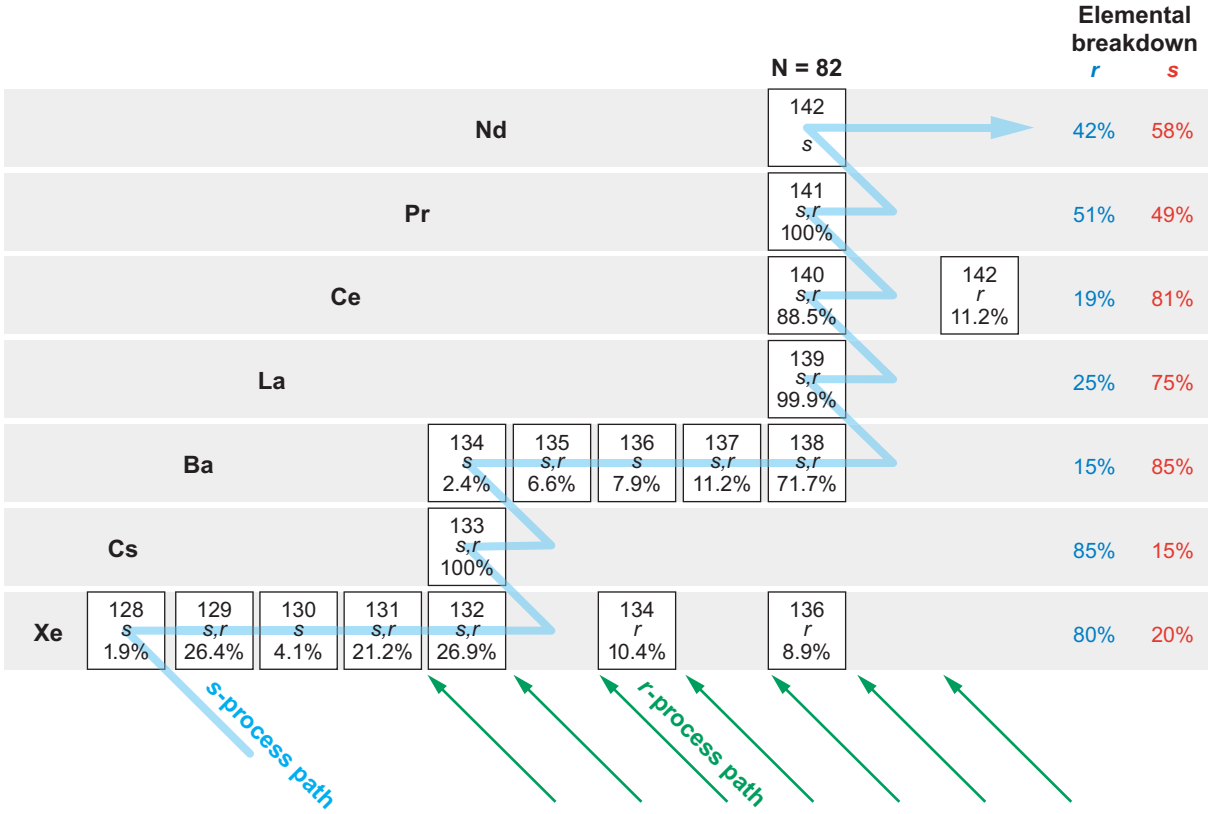

Figure 2

A portion of the nuclear chart showing elements Xe to Pr and the production of each isotope by the *p*-, *s*-, and *r*-processes. The *s*-process (*light blue line*) operates close to stability—the black boxes show stable nuclei—whereas the *r*-process is formed out of very neutron-rich (unstable) nuclei that β decay back (*green lines*) to stability. We also add one isotope of Nd to this chart to indicate the next steps in the *s*-process chain, but do not indicate the other Nd isotopes. Listed to the outside right are the total percentage breakdowns by process for each element.

additional "weak" component (coming from He core fusion in massive stars) is needed to account for *s*-nuclei with A $\leq$ 88, and a "strong" component is suggested to account for roughly 50% of Solar ^{208}Pb (Clayton & Rassbach 1967, Käppeler et al. 1982).

The general rules for the *s*-process describe well situations where τ_n is very different than τ_β. But an unstable nuclide with $\tau_n \sim \tau_\beta$ along the *s*-path suffers partly from both *n*-capture and β decay. There are important "branching points" along the *s*-path that depend on neutron density and/or temperature, by increased β-decay rates as a result of increased thermal populations of low-lying nuclear states, or by the pulsed nature of the *s*-process in asymptotic giant branch (AGB) stars (e.g., Käppeler et al. 1990). An example is ^{141}Ce, which at high neutron density becomes a branching point in the *s* path, partly feeding ^{142}Ce via the neutron capture channel and partly ^{141}Pr via the β-decay channel. The effect of this branching is also to partly bypass the *s*-only ^{142}Nd. Continued pursuit of accurate experimental cross sections are essential steps in producing the most realistic *s*-process yields from AGB models stars.

On the neutron-rich side, there are stable isotopes that cannot be fed by the *s*-process because they are preceded by an unstable isotope of short half-life. In **Figure 2** these isotopes are ^{134}Xe

and ^{136}Xe; they will be called *r*-only. In between, there are stable "*s*, *r*" isotopes that can be fed by both the *s*-process and the *r*-process (e.g., ^{135,137}Ba in **Figure 2**), and these must be considered on a case-by-case basis. For example, ^{138}Ba is officially an *s*, *r* nuclide, but it is neutron magic (N = 82) and has a very low *n*-capture cross section with respect to the adjacent nuclides. This means that ^{138}Ba builds up during the *s*-process, resulting in a mostly *s*-process origin. Similar behavior applies to other neutron-magic isotopes.

Some lighter proton-rich isotopes are not depicted in **Figure 2**: ^{124,126}Xe, ^{130,132}Ba, ^{136,138}Ce. These are the so-called *p*-nuclei, which were defined by Burbidge et al. (1957) as relatively proton-rich isotopes that are synthesized in (p, γ) and/or (γ, n) reactions. More generally, these nuclei can be classified as bypassed nuclei that are shielded from creation in any *n*-capture synthesis path. These *p*-nuclei are very minor contributors to their elemental abundances: 0.1–0.2% of the totals are typical. Presence of *p*-nuclei can only be determined in meteoritic isotopic investigations. Detailed discussions of *p*-nuclei have been given in the reviews of, e.g., Lambert (1992) and Arnould & Goriely (2003) and these isotopes will not be considered further here.

Neutron number densities or fluxes are very different in the *s*- and *r*-process. For the *s*-process typical values are ($n_n < \sim 10^8$ cm^{-3}, e.g., Busso, Gallino & Wasserburg 1999). Far larger values of 10^{24}–10^{28} cm^{-3} are typical of the *r*-process (Kratz et al. 2007, and references therein). This radical density contrast demands very different astrophysical environments for *s*- and *r*-process element synthesis. Decades of astronomical observations have cataloged stars that clearly have been enriched with *s*-process elements. A famous early example was Merrill's (1952) identification of radioactive Tc ($\tau_{1/2} = 2.1 \times 10^5$ years for *s*-process isotope ^{99}Tc) in *n*-capture-rich S stars. This work showed that such *n*-capture elements can be synthesized in situ by quiescently evolving stars. Theoretical studies have led to the identification of the *s*-process site in low- to intermediate-mass stars (i.e., $M \simeq 1.3 - 8\,M_\odot$) during the red giant, specifically the AGB phase. (See the reviews by Busso, Gallino & Wasserburg 1999; Straniero et al. 2003; Busso et al. 2004; Herwig 2005; Straniero, Gallino & Cristallo 2006.)

The large neutron number densities required for the *r*-process argue for an explosive environment. Burbidge et al. (1957) and Cameron (1957a,b) first suggested that the site was the neutron-rich regions outside of a nascent neutron star formed in a supernova explosion. Unfortunately, the details of dynamical supernova events (e.g., the neutrino interactions with matter and the equation of state of ultradense matter) are quite complicated. Furthermore, in contrast to the *s*-process, there have been no observational detections of in situ *r*-process-elements in supernovae or their remnants. Nevertheless, much circumstantial evidence and models argue for a supernova *r*-process origin. A promising model is that of the neutrino-wind, a stream of particles created by neutrinos shortly after the supernova explosion (see, e.g., Woosley et al. 1994, Takahashi, Witti & Janka 1994, Terasawa et al. 2002, Wanajo et al. 2002, Thompson 2003). Despite the promise of this model, theoretical problems remain (e.g., difficulties in obtaining a successful supernova explosion, lack of sufficient entropy to synthesize the heaviest nuclei, etc.) that prevent a definitive confirmation of this site with *r*-process nucleosynthesis. See Cowan & Thielemann (2004), and references therein, for a more detailed discussion of *r*-process nucleosynthesis in supernovae.

Over the years alternative models have been suggested for *r*-process synthesis, including binary neutron star or black hole mergers (Lattimer et al. 1977; Rosswog et al. 1999; Freiburghaus, Rosswog & Thielemann 1999; but see also Argast et al. 2004), prompt explosions of low-mass supernovae (Mathews & Cowan 1990; Mathews, Bazan & Cowan 1992; Wheeler, Cowan & Hillebrandt 1998; Ishimaru & Wanajo 1999; Wanajo et al. 2003; Ning, Qian & Meyer 2007) or accretion-induced collapse models (e.g., Cohen et al. 2003, Qian & Wasserburg 2003), and bubbles or jets produced during supernova explosions (LeBlanc & Wilson 1970; Cameron 2001,

2003; see also the recent *r*-process review by Arnould, Goriely & Takahashi 2008). Regrettably, none of these models has been entirely successful in synthesizing the total abundance distribution of *r*-process nuclei seen in nature. Thus, though much work has been done to understand how the *r*-process operates, its astrophysical sites have still not been confirmed (but see Section 6.2 for further discussion of this issue).

3. SOLAR-SYSTEM ABUNDANCES

The Solar-system abundance distribution has been investigated repeatedly for more than a century. The first comprehensive evaluation was done by Suess & Urey (1956; see their paper for reviews of earlier studies). **Figure 3** compares the early work of Cameron (1959) to the recent compilation of Lodders (2003). It illustrates isotopic number-density abundances on the meteoritic scale ($N_{Si} = 10^6$) as a function of mass number. Additional Solar-system compilations include those of Anders & Grevesse (1989), Grevesse & Sauval (1998), and Grevesse, Asplund & Sauval (2007). The Cameron and Lodders Solar-system abundances agree qualitatively very well, as do the other studies. The broad outlines of Solar-system abundances have been understood for decades.

Breakdowns of Solar-system isotopic abundances into *s*-, *r*-, and *p*-process components have been done by a number of researchers, beginning with the pioneering study of Cameron (1973). Such analyses usually involve first determining the *s*-process contributions. As discussed in Section 2, the classical approach is to fit the σN_s for nuclei lying along the *s*-process path for nuclides far from neutron-magic nuclei to the Solar-system abundances of *s*-only nuclei, and then the *s*-process contributions to other nuclei are determined by subtraction of this curve from the total Solar-system abundances. In this manner, and having first experimentally obtained σ, the *s*-process

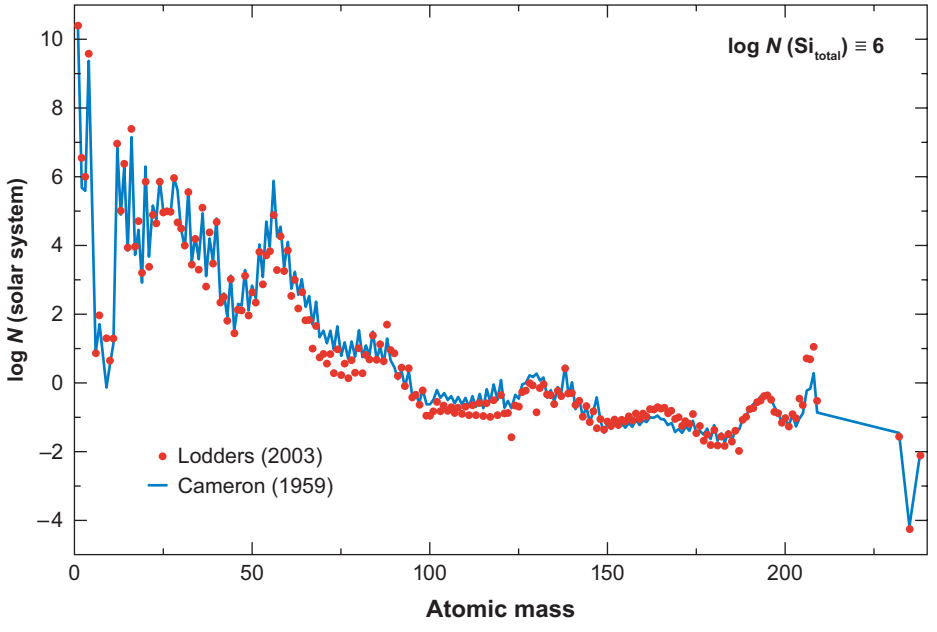

Figure 3

The total Solar-system abundances by mass number based upon the Si $= 10^6$ (meteoritic) scale. Comparison is made between the early work of Cameron (1959) (*filled red circles*) and the more recent compilation by Lodders (2003) (*solid blue line*).

abundances in Solar-system material have been estimated by, e.g., Käppeler, Beer & Wisshak (1989), Arlandini et al. (1999), Burris et al. (2000), Simmerer et al. (2004), and Cowan & Sneden (2006). We show a Solar-system isotopic abundance breakdown in **Table 1**, based on the classical *s*-process model (see also Cowan & Sneden 2006).

The classical model approach reproduces the abundances of most *s*-process nuclei, including shielded ones, and is independent of any stellar model assumptions, but it ignores the details of nuclear structure, which can affect the *s*-process path and hence those computed abundances. An alternative approach has employed theoretical models of the conditions expected to occur in the partial He-fusion zones of AGB stars that are the sites of the main and strong component of the *s*-process (Arlandini et al. 1999, Travaglio et al. 2004). Again employing the experimentally determined neutron-capture cross sections, Arlandini et al. have predicted a set of *s*-process abundances based on the stellar model.

Because the heavy-element abundances in Solar-system material are sums of the two *n*-capture processes, knowing the *s*-process contributions allows the determination of the *r*-process contributions, or residuals, for individual isotopes (Käppeler, Beer & Wisshak 1989, Arlandini et al. 1999, Cowan & Sneden 2006). Summations of the isotopic contributions by individual *n*-capture process then yield elemental Solar-system *s*- and *r*-only abundance distributions. These in turn can be compared with stellar, particularly metal-poor halo star, abundances. Such comparisons can provide enormous insight into a wide range of problems and areas of interest to astronomy and astrophysics, as we discuss in succeeding sections. For the Xe-Pr elements of **Figure 2**, we note for each isotope the total Solar-system elemental percentage of that isotope. We also list, to the right of the each element's isotopes, the percentage breakdown by process of that elemental abundance in Solar-system material. It is seen, for example, that Xe and Cs are dominated by the *r*-process, whereas Ba and La are made mainly by the *s*-process. The total Solar-system $Z > 30$ element content is produced in roughly equal amounts by the two *n*-capture processes. No evidence has emerged for the existence of substantial *n*-capture abundance contributions by neutron density regimes intermediate between those of the *s*- and *r*-process.

4. THE *r*-PROCESS: OBSERVATIONS

The existence of very metal-poor stars enriched in the *r*-process elements was observationally established by Spite & Spite (1978). They reported abundances for several low-metallicity [we adopt the standard spectroscopic notation (Helfer, Wallerstein & Greenstein 1959) that for elements A and B, $\log \varepsilon(\mathrm{A}) \equiv \log_{10}(\mathrm{N_A/N_H}) + 12.0$, and $[\mathrm{A/B}] \equiv \log_{10}(\mathrm{N_A/N_B})_* - \log_{10}(\mathrm{N_A/N_B})_\odot$; also, metallicity is defined as the stellar [Fe/H] value] bright stars ([Fe/H] < -2), finding several examples with [Eu/Fe] ≥ 0 and [Eu/Ba] > 0.5. Spite & Spite (1978) also included HD 122563 in their program. They confirmed the earlier result of Pagel (1965), based on a reanalysis of equivalent width data of Wallerstein et al. (1963), that this brightest of all very metal-poor stars has some *n*-capture deficiencies but a large [Eu/Ba] value (the *n*-capture abundance pattern of HD 122563 was considered in more detail by Sneden & Parthasarathy 1983, and a comprehensive study has been published recently by Honda et al. 2006). Truran (1981) used these results and earlier studies of other stars with [Ba/Fe] $\lesssim -0.5$ (e.g., Peterson 1976 and references therein) to argue that "the observed trends follow in a natural and straightforward manner from the assumption that the Y and Ba [as well as Eu] in the most extreme metal-poor stars represent products of *r*-process nucleosynthesis." A high-resolution spectroscopic analysis of HD 115444 by Griffin et al. (1982) revealed the first example of substantial *n*-capture overabundances at very low metallicities; a subsequent study by Westin et al. (2000) showed that the *n*-capture element distribution of HD 115444 matches a scaled Solar *r*-process pattern very well.

Table 1 Solar-system isotopic abundance breakdowns by *s*- and *r*-process

Element	Z	Isotope	N[s]	N[r]	Element	Z	Isotope	N[s]	N[r]
Ga	31	69	11.137	11.600	Pd	46	104	0.165	0.000
		71	10.413	4.700			105	0.040	0.269
Ge	32	70	15.000	0.000			106	0.186	0.193
		72	18.323	14.000			108	0.226	0.145
		73	3.531	5.670			110	0.000	0.163
		74	15.733	27.300	Ag	47	107	0.058	0.239
		76	0.000	9.200			109	0.059	0.196
As	33	75	1.456	5.330	Cd	48	110	0.178	0.000
Se	34	76	4.656	0.000			111	0.042	0.165
		77	1.679	3.040			112	0.198	0.196
		78	7.402	7.210			113	0.060	0.139
		80	7.446	24.300			114	0.287	0.140
		82	0.000	5.710			116	0.000	0.121
Br	35	79	0.450	0.000	In	49	115	0.057	0.121
		81	0.479	4.640	Sn	50	116	0.511	0.000
Kr	36	80	1.021	0.000			117	0.146	0.128
		82	6.207	0.000			118	0.706	0.137
		83	1.989	3.750			119	0.155	0.065
		84	10.575	18.000			120	1.099	0.078
		86	9.481	0.930			122	0.000	0.154
Rb	37	85	0.690	2.790			124	0.000	0.199
		87	2.214	0.100	Sb	51	121	0.047	0.113
Sr	38	86	2.111	0.000			123	0.000	0.132
		87	1.443	0.000	Te	52	122	0.133	0.000
		88	16.986	2.550			123	0.047	0.000
Y	39	89	3.344	1.310			124	0.248	0.000
Zr	40	90	4.529	0.990			125	0.088	0.267
		91	1.158	0.040			126	0.450	0.525
		92	1.289	0.540			128	0.000	1.526
		94	1.687	0.170			130	0.000	1.634
		96	0.000	0.300	I	53	127	0.050	0.851
Nb	41	93	0.229	0.110	Xe	54	128	0.126	0.000
Mo	42	95	0.189	0.213			129	0.066	1.240
		96	0.475	0.000			130	0.199	0.000
		97	0.156	0.087			131	0.087	0.954
		98	0.514	0.093			132	0.498	0.800
		100	0.000	0.242			134	0.000	0.449
Ru	44	99	0.049	0.000	Cs	55	133	0.056	0.315
		100	0.242	0.000	Ba	56	134	0.178	0.000
		101	0.050	0.266			135	0.068	0.298
		102	0.261	0.327			136	0.500	0.000
		104	0.000	0.348			137	0.372	0.283
Rh	45	103	0.055	0.289			138	3.546	0.225

(*Continued*)

Table 1 (*Continued*)

Element	Z	Isotope	N[s]	N[r]	Element	Z	Isotope	N[s]	N[r]
La	57	139	0.337	0.110	Lu	71	175	0.006	0.031
Ce	58	140	0.894	0.089			176	0.002	0.000
		142	0.000	0.115	Hf	72	176	0.008	0.000
Pr	59	141	0.079	0.082			177	0.005	0.024
Nd	60	142	0.227	0.000			178	0.021	0.022
		143	0.037	0.065			179	0.007	0.015
		144	0.105	0.094			180	0.035	0.020
		145	0.020	0.049	Ta	73	181	0.009	0.013
		146	0.091	0.053	W	74	182	0.024	0.012
		148	0.004	0.044			183	0.013	0.007
		150	0.000	0.047			184	0.029	0.013
Sm	62	147	0.003	0.031			186	0.006	0.031
		148	0.038	0.000	Re	75	185	0.004	0.014
		149	0.005	0.031			187	0.001	0.033
		150	0.022	0.000	Os	76	186	0.012	0.000
		152	0.018	0.053			187	0.006	0.000
		154	0.000	0.059			188	0.016	0.079
Eu	63	151	0.000	0.042			189	0.004	0.111
		153	0.002	0.048			190	0.021	0.168
Gd	64	152	0.001	0.000			192	0.001	0.293
		154	0.009	0.000	Ir	77	191	0.005	0.241
		155	0.003	0.045			193	0.003	0.408
		156	0.015	0.055	Pt	78	192	0.010	0.000
		157	0.007	0.046			194	0.020	0.431
		158	0.027	0.058			195	0.006	0.457
		160	0.000	0.072			196	0.035	0.312
Tb	65	159	0.004	0.060			198	0.000	0.099
Dy	66	160	0.009	0.000	Au	79	197	0.010	0.176
		161	0.004	0.075	Hg	80	198	0.035	0.000
		162	0.016	0.101			199	0.016	0.043
		163	0.002	0.093			200	0.051	0.030
		164	0.018	0.091			201	0.020	0.027
Ho	67	165	0.006	0.083			202	0.079	0.026
Er	68	164	0.004	0.000			204	0.000	0.020
		166	0.012	0.072	Tl	81	203	0.042	0.012
		167	0.005	0.053			205	0.060	0.041
		168	0.020	0.047	Pb	82	204	0.057	0.000
		170	0.001	0.037			206	0.326	0.223
Tm	69	169	0.006	0.031			207	0.313	0.280
Yb	70	170	0.006	0.000			208	1.587	0.118
		171	0.004	0.029	Bi	83	209	0.051	0.093
		172	0.018	0.036	Th	90	232	0.000	0.042
		173	0.008	0.031	U	92	235	0.000	0.006
		174	0.040	0.037			238	0.000	0.020
		176	0.000	0.030					

Metal-poor *r*-process-rich (hereafter *r*-rich) stars increased in importance with the discovery of very strong rare-earth transitions in CS 22892-052. This very low-metallicity star ([Fe/H] ~ -3; Beers, Preston & Shectman 1992) was included in the high-resolution survey of McWilliam et al. (1995). It was singled out for special study by Sneden et al. (1994) and has been reinvestigated repeatedly (e.g., Sneden et al. 2003 and references therein; Barklem et al. 2005). All these studies confirm the *r*-process signature of CS 22892-052: [Eu/Fe] $\simeq +1.6$ and [Eu/Ba] $\simeq +0.7$.

Several other extremely *r*-rich stars have been identified and studied in detail, e.g., CS 31082-001 (Hill et al. 2002), CS 22183-031 (Honda et al. 2004), and HE 1523-0901 (Frebel et al. 2007). Such stars are labeled *r*-II by Christlieb et al. (2004), defined as those very metal-poor ([Fe/H] $\lesssim -2.5$) stars with [Eu/Fe] $> +1.0$ and [Eu/Ba] < 0.0. A few other stars, such as BD+17 3248 (Cowan et al. 2002) and CS 30306-132 (Honda et al. 2004), that would formally be classified in this system as *r*-I ($+0.3 \leq$ [Eu/Fe] $\leq +1.0$ and [Eu/Ba] < 0.0) are nearly as *r*-rich.

A common thread connects the *r*-II discoveries: They can only be found through high-resolution spectroscopy. The clearest signature of stellar *r*-process-richness is an anomalously large Eu abundance. However, the handful of available Eu II transitions cannot be easily detected in low-resolution spectra. We illustrate this in **Figure 4** by comparing the spectra of CS 22892-052 and the *n*-capture-weak star HD 122563. These two stars have similar atmospheric parameters: for CS 22892-052, $T_{\rm eff}$, log *g*, [Fe/H] = 4800 K, 1.5, -3.1 (Sneden et al. 2003), and for HD 122563, 4500 K, 1.3, -2.7 (Westin et al. 2000). Inspection of the low-resolution ($R \equiv \lambda/\Delta\lambda \sim 2500$) spectra in the top panel suggests that both stars are cool and metal-poor, and that CS 22892-052 has a relatively strong CH G-band. Closer examination of a small portion of these same spectra in the middle panel reveals slightly stronger absorption in CS 22892-052 at several wavelengths, in particular near 4130 Å. But only detailed high-resolution ($R \simeq 45{,}000-60{,}000$) spectra of these two stars reveals their true differences in line strengths: While HD 122563 has deeper Fe-peak lines owing to its lower temperature and higher metallicity, CS 22892-052 exhibits strong *n*-capture lines that are weak or entirely absent in the other star. These two stars were deliberately chosen for the extremely large *r*-process abundance contrast; milder examples will be undetectable at low spectral resolution.

To systematically identify more *r*-rich stars, Christlieb et al. (2004) gathered "snapshot" moderately high-resolution ($R \sim 20{,}000$) and signal-to-noise (S/N ~ 50) spectra of stars identified in their low-resolution Hamburg-ESO low-metallicity survey. Of 253 stars with abundances reported by Barklem et al. (2005), they found that about 17% are *r*-process enhanced (8 new *r*-II and 35 new *r*-I stars). The *r*-II *n*-capture abundance patterns closely mimic those of the more well-known CS 22892-052 and CS 31082-001. This survey and others like it take substantial large-telescope resources but are the only way that significant numbers of *r*-rich stars can be identified.

Almost all *r*-rich stars discovered to date have been red giants. We illustrate this in the left-hand Hertzsprung-Russell (HR) diagram of **Figure 5**. Only three stars have parameters that place them below the base of the first-ascent giant branch. The cause probably is an observational one: Warm near-main-sequence stars simply have much weaker-lined spectra than cool giants with the same chemical compositions. Lines of Eu II are often undetectable in the warmer stars even when the Eu abundances are relatively high. Establishing the true fraction of warm low-metallicity stars with *r*-process enhancements will require much larger high-resolution spectroscopic surveys.

The *r*-II giant spectra are goldmines of information about *n*-capture elements. Their low $T_{\rm eff}$, log *g*, and [Fe/H] values combine with order-of-magnitude *n*-capture overabundances to render many obscure elements easily accessible for detailed study. More than 30 *n*-capture elements have been detected in several of these stars, including essentially all stable rare-earth elements in a couple of cases. Elements such as Tb and Ho can have more reliably determined abundances in these stars than in the Sun. A major factor in the increased accuracy of *n*-capture abundances has been the significant upgrade in the quality of input atomic data—transition probabilities, hyperfine

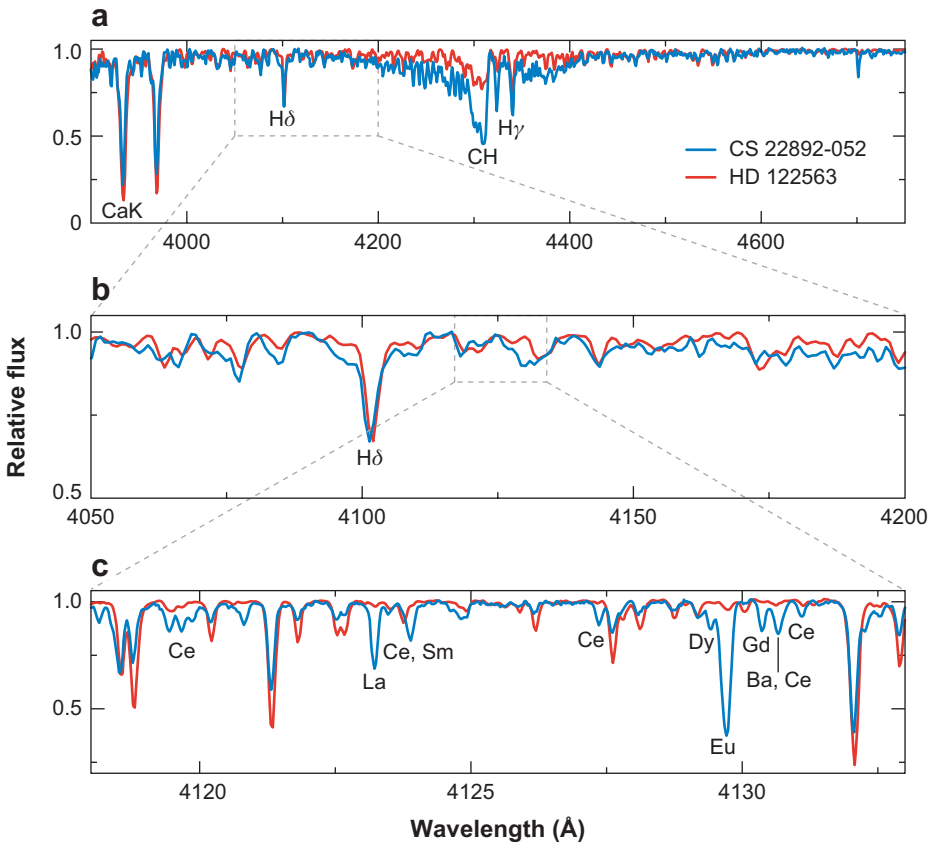

Figure 4

Spectra of the *r*-process-rich star CS 22892-052 (*blue line*) contrasted with spectra of the *n*-capture-deficient star HD 122563. In panel a, relatively low-resolution (R ∼ 2500) spectra from the Rossi et al. (2005) survey, covering most of the standard stellar classification wavelength region, are displayed. The carbon-richness ([C/Fe] ∼ +1) of CS 22892-052 is apparent in its CH band strength. An expanded view of a smaller portion of these spectra is shown in panel b. High-resolution spectra of an even narrower wavelength region are shown in panel c. The data for CS 22892-052 and HD 122563 are those of Sneden et al. (2003) and Westin et al. (2000), respectively.

splitting constants, and isotopic wavelength shifts. Several groups, especially those in Liège, Lund, and Wisconsin, have been producing the requisite laboratory and theoretical atomic data over the past couple of decades. Summaries of these efforts are in Wahlgren (2002) and Biémont & Quinet (2003). Transition probability data of particular relevance to metal-poor *r*-rich stars continue to improve (e.g., Den Hartog et al. 2006, Lundqvist et al. 2006, Malcheva et al. 2006, Xu et al. 2006, Lawler et al. 2006). With enough transitions of a species available for abundance analysis, and modern atomic data, it is now possible to determine relative abundances of many *n*-capture elements (like [La/Eu], [Hf/Zr]) to accuracies of $\sim \pm 0.05$ dex. Note that Barium ($Z = 56$) is usually considered together with the rare-earth elements. With five strong transitions, 4554 Å (most often employed), 4934 Å, 5853 Å, 6141 Å, and 6496 Å, it has been a convenient indicator of *n*-capture element abundance, and it will be so employed later in this review. However, caution is warranted as it is difficult to derive accurate abundances for this element. Barium has five isotopes whose production fractions in the *r*-process and *s*-process are significantly different. Derived

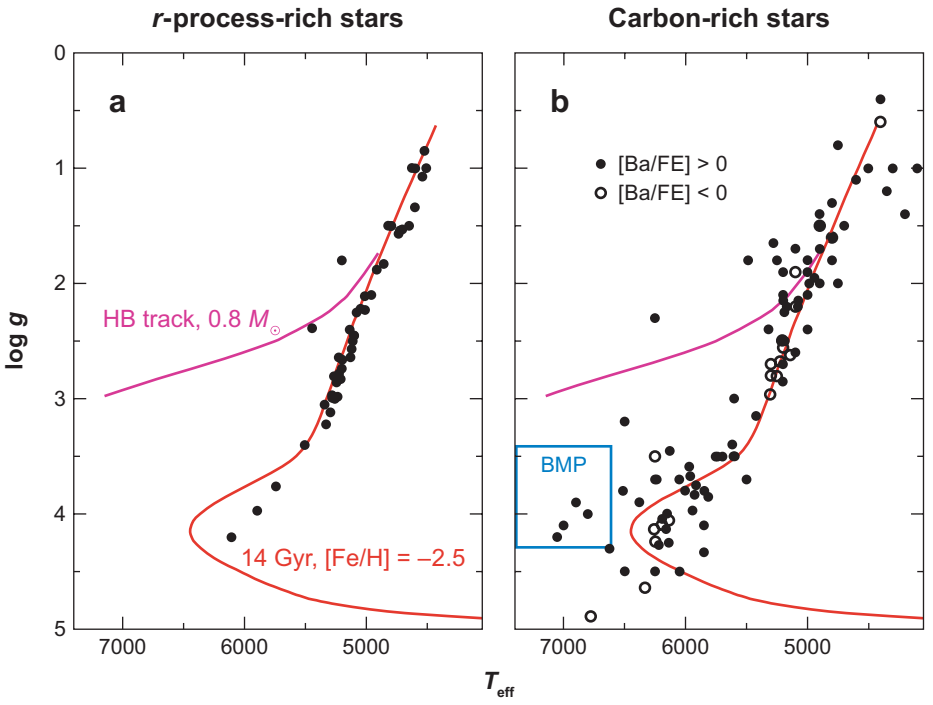

Figure 5

(*a*) Hertzsprung-Russell diagrams for *r*-process-rich stars and (*b*) carbon-rich stars (both *s*-process-weak and *s*-process-strong types). Most of the *r*-process data are from Barklem et al. (2005), with the addition of data from Westin et al. (2000), Cowan et al. (2002), Hill et al. (2002), Johnson (2002), Sneden et al. (2003), Honda et al. (2004), Ivans et al. (2006), and Frebel et al. (2007). Sources of the C-rich stars are from a few large-sample surveys (Van Eck et al. 2003; Cohen et al. 2004, 2006; Barklem et al. 2005; Aoki et al. 2007a, and references therein), supplemented by many papers on individual stars. The complete list of references to the points for the C-rich stars is given in Sneden & Lawler (2008). For illustration we have added a 14-Gyr isochrone (*red line*; Demarque et al. 2004), and a 0.8-$M_{\odot}$ metal-poor star horizontal-branch evolutionary track (*magenta line*; Cassisi et al. 2004).

Ba abundances from the 4554 and 4934 Å lines are very sensitive to the assumed *r/s* fraction. Additionally, these two lines are often strong enough to be on the damping part of the curve of growth. In this case, the lines are formed relatively far out in the atmosphere and are probably afflicted with departures from local thermodynamic equilibrium. Traditional analytical methods here yield abundances with heightened uncertainties.

In **Figure 6** we illustrate the abundance improvements resulting from the improved lab data. In this figure, originally published abundances for three *r*-rich stars are contrasted with revised abundances that have accompanied the publication of new transition probabilities. It is clear that the revised abundances of these *r*-rich stars have substantially smaller uncertainties, and their abundance ratios with respect to the normalization element Eu more closely match each other. Over the larger *n*-capture element domain, the relative abundance ratios are similarly reliable for all elements that have transitions arising from low excitation states of their ionized species. However, this generally includes only a few elements outside the $56 \leq Z \leq 72$ regime: Sr, Y, Zr, Nb, Th, and U.

The spectroscopic situation is less sanguine for the remaining *n*-capture elements. Significant gaps in elements unobserved in very metal-poor stars exist for the atomic number intervals

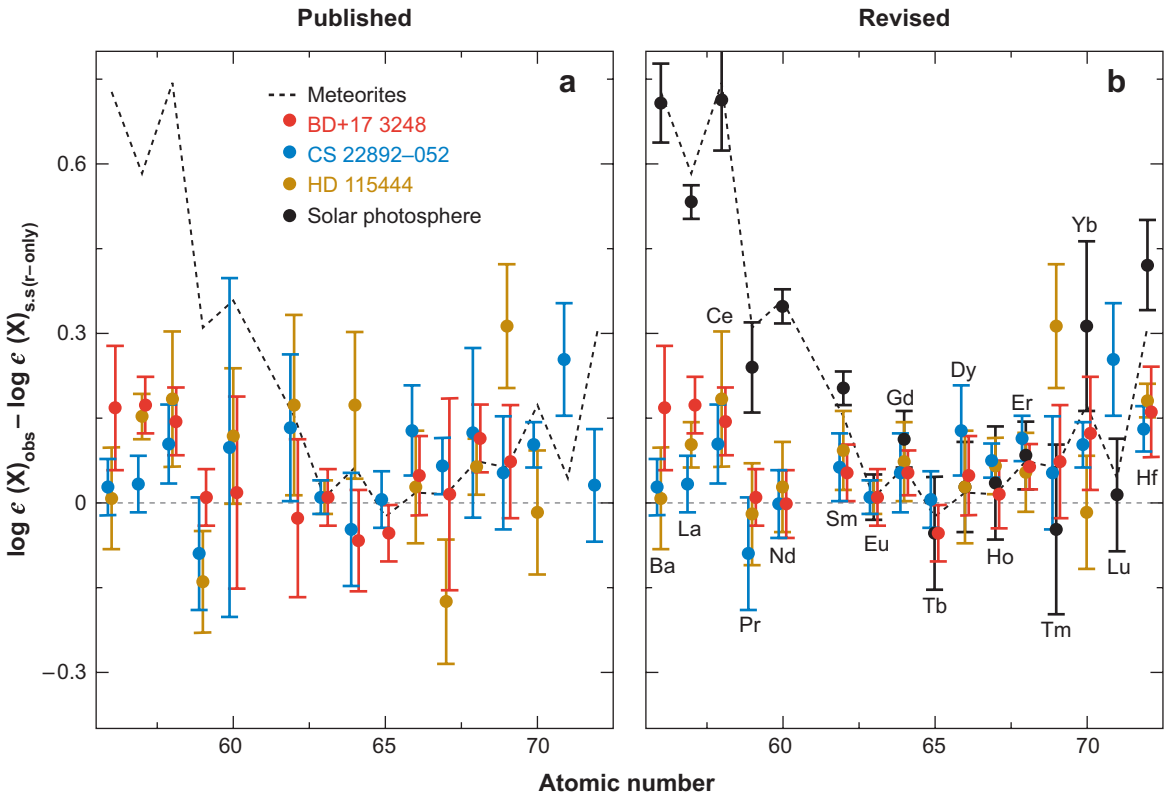

Figure 6

(*a*) Abundances of meteorites (Lodders 2003), CS 22892-052 (Sneden et al. 2003), HD 115444 (Westin et al. 2000), and BD+17 3248 (Cowan et al. 2002) minus Solar-system *r*-process-only abundances (Simmerer et al. 2004), with abundance differences normalized to zero at Eu. (*b*) Corrected abundance differences for the three *r*-process-rich stars and the Solar photosphere after application of recent laboratory transition probabilities (Lawler et al. 2007, and references therein). This figure is an update of figure 5 of Den Hartog et al. 2006, in which a more detailed description of the figure can be found.

Z = 33–37, 48–55, and 73–75. Many elements (e.g., As, Te) have strong transitions only deep in the vacuum ultraviolet (UV). Other elements (e.g., Ge, Ru, Rh, Ag, Ir) present a few lines accessible to ground-based telescopes, but in general they occur in the very crowded near-UV spectral region (3000–4000 Å). Their detectable lines are generally from the neutral species, so large Saha corrections are often required to derive elemental abundances. Abundance uncertainties are thus larger for these elements than they are for those with lots of ionized-species transitions in the blue-yellow spectral domains. The problems are illustrated by platinum (Z = 78), which is a relatively abundant third *r*-peak element. Five Pt I lines were identified in the Solar spectrum by Moore, Minnaert & Houtgast (1966). However, Den Hartog et al. (2005) found that of these only the 3064 Å line can be used to measure Pt abundances in metal-poor stars, and then only in the most *n*-capture-rich cases. All other useful Pt I transitions occur below 3000 Å (see Cowan et al. 2005), accessible only to high-resolution UV spectrographs on satellites. No such instruments are currently in working order.

These concerns however cannot completely explain the star-to-star scatter of lighter *n*-capture elements with respect to the heavier Z ≥ 56 elements. Some large-sample studies comparing the Sr-Y-Zr element group with the rare-earth elements have highlighted this issue. For example,

Johnson & Bolte (2002b) show that variations in [Y/Ba] increase with decreasing metallicity, reaching nearly 1.5 dex at [Fe/H] ~ -3. Aoki et al. (2005) extend these arguments with a different stellar sample, demonstrating that the light/heavy scatter is larger in stars with smaller overall *n*-capture enrichment. These variations are evident also in the low-metallicity globular cluster M15 ([Fe/H] ~ -2.5). The *n*-capture abundances of globular clusters (typically more metal-rich than of interest here) generally agree with those of field stars at similar metallicities (e.g., as reviewed in Gratton, Sneden & Carretta 2004). In M15 a nearly pure *r*-process abundance signature for Ba and heavier elements is observed (Sneden et al. 2000b), but also a large star-to-star variation in their total content with respect to the Fe-group (the [Eu/Fe] ratio ranges from +0.1 to +0.8; Sneden et al. 1997). Recently, Otsuki et al. (2006) have discovered that light/heavy abundance ratios such as [Y/Eu] are anticorrelated with the [Eu/Fe] (or [Eu/H]) general *r*-process abundance enrichment. This *r*-process complexity will be discussed further in Section 6.2.

5. THE *s*-PROCESS: OBSERVATIONS

Low-metallicity stars with large *s*-process abundances are relatively easy to identify. The *s*-process is mainly a byproduct of partial helium burning. Its main yield is carbon. Very metal-poor stars with substantial carbon overabundances can be spotted in low-metallicity spectra through the wide absorption troughs of CH, CN, and sometimes C_2 molecular bands. Examples of metal-poor, C-rich stellar spectra are shown in figures 9 and 12 of Beers, Preston & Shectman (1992), and figure 1 of Rossi et al. (2005). Very C-rich stars ([C/Fe] $\geq +1.0$) comprise a substantial fraction of very metal-poor stars, with estimates ranging from $14 \pm 4\%$ (Cohen et al. 2005) to $21 \pm 2\%$ (Lucatello et al. 2006) for stars with [Fe/H] ≤ -2.0. The fraction of C-rich stars probably increases with decreasing metallicity, but better statistics are needed to clarify this issue.

Because C-rich stars can be found with relative ease, many of them have enjoyed high-resolution abundance studies. We show their HR diagram locations in **Figure 5*b***. Here we used open circles to represent 21 C-rich stars that have no apparent *n*-capture overabundances, using the [Ba/Fe] value, determined in nearly all studies, as a surrogate for the whole *n*-capture element group. The 90 others that are *n*-capture-rich by this criterion are denoted with filled circles. Division of the two groups at [Ba/Fe] $= 0$ is arbitrary, but 84/90 of the barium-enhanced stars actually have [Ba/Fe] $> +0.5$. They are truly *n*-capture-rich. Because the main interest of this review is *n*-capture elements, the barium-weak stars will not be considered further.

The *n*-capture abundance distribution of the C- and Ba-rich stars is nearly always characteristic of the *s*-process: [Ba/Eu] > 0. Lighter rare-earth elements (e.g., La and Ce) tend to be more overabundant than heavier ones (e.g., Gd and Dy). However, the unique signature of low-metallicity *s*-rich stars is the often extreme overabundance of Pb. This element has only a few spectral features. Observers typically concentrate only on the Pb I 4057.8 Å transition, which goes undetected in most metal-poor stars. However, Gallino et al. (1998) and Goriely & Mowlavi (2000) used *s*-process synthesis calculations to predict large Pb abundances in low-metallicity He-fusion environments. Van Eck et al. (2001, 2003) reported discovery of strong Pb I 4057 Å lines in several metal-poor CH stars. Those researchers and others (e.g., Aoki et al. 2002c, Cohen et al. 2006) have found a large spread in [Pb/Ba] among the *s*-rich stars.

Low-metallicity *s*-rich stars (called carbon-enhanced metal-poor *s*-process-rich, or CEMP-*s*) exhibit very large Ba-to-Sr ratios. These elements are representative of so-called hs and ls *n*-capture element groups and have very strong transitions in cool stars. In **Figure 7**, we correlate [Ba/Sr] values with [Ba/Fe] (a measure of bulk *n*-capture enhancement). Broad categories of [C/Fe] abundance ratios are denoted by symbol colors. The [Ba/Sr] ratios generally increase with increasing [Ba/Fe]. This suggests that the increases in both quantities are caused by addition of Ba rather

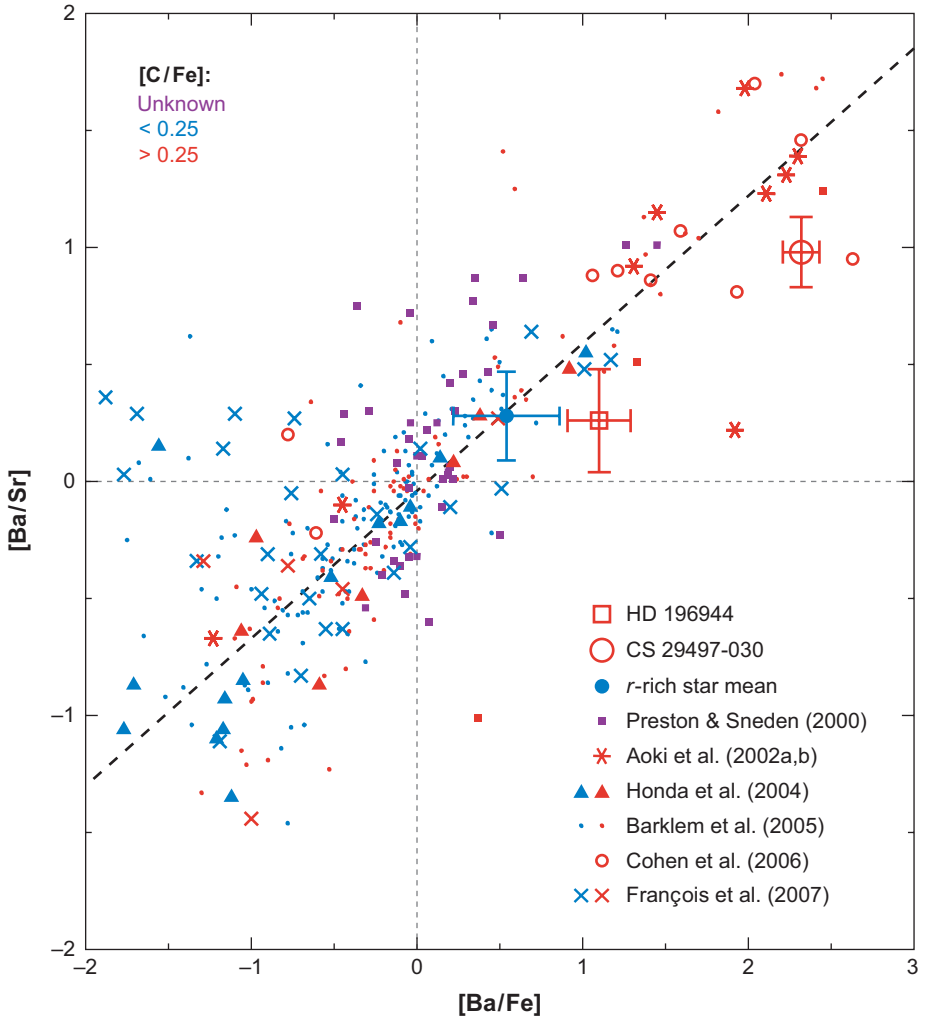

Figure 7

Ba/Sr abundance ratios as a function of Ba/Fe in metal-poor stars. Most data are taken from selected large-sample surveys such as Preston & Sneden (2000, *filled squares*), Honda et al. (2004, *filled triangles*), Barklem et al. (2005, *dots*), Cohen et al. (2006, *open circles*), and François et al. (2007, *crosses*). The Pb-rich stars HD 196944 (Van Eck et al. 2001, Aoki et al. 2002c) and CS 29497-030 (Ivans et al. 2005) are indicated by a large open square and circle, respectively. The mean of 16 very *r*-rich stars ([Eu/Fe] > 0.80; Westin et al. 2000, Cowan et al. 2002, Hill et al. 2002, Sneden et al. 2003, Honda et al. 2004, Barklem et al. 2005, Ivans et al. 2006) is indicated with a filled circle, whose error bars are the σ values of the mean [Ba/Sr] and [Ba/Fe] values. The colors of the points designate the carbon richness, as indicated in the figure legend; purple is unknown, blue is [C/Fe] < 0.25, and red is [C/Fe] > 0.25. The dashed line is an approximate best fit to the main trend of data.

than destruction of Sr. The *r*-rich stars, of course, also have large Sr and Ba abundances, but they do not rival the CEMP-*s* stars. The most extreme *r*-rich example is CS 29497-004 ([Ba/Fe] = +1.21 and [Ba/Sr] = +0.64; Barklem et al. 2005), and the mean values for 16 very *r*-rich stars are [Ba/Fe] = +0.54 and [Ba/Sr] = +0.28. The largest Ba and Sr abundances occur in the CEMP-*s* stars. These are the stars with hugely enhanced Pb abundances.

About half of the known CEMP-*s* stars with measured Eu abundances are also *r*-process rich, defined here as [Eu/Fe] > 1. Among them are several stars with [Eu/Fe] ∼ +2, higher than the ratio in the most *r*-rich stars: HE 2148-1247 (Cohen et al. 2003), the first CEMP-(*s* + *r*) discovered, CS 29497-030 (Ivans et al. 2005), HE 0338-3945 (Jonsell et al. 2006), CS 22898-027 (Preston & Sneden 2001, Aoki et al. 2002c), HE 1305+0007 (Goswami et al. 2006), and HE 1105+0027 (Barklem et al. 2005). The nucleosynthesis histories of such stars must be complex amalgams of contributions of high- and low-mass prior donor stars.

A few "blue metal-poor" stars (Preston, Beers & Shectman 1994; Preston & Sneden 2000) also are C- and *s*-rich. These stars are halo field counterparts to cluster blue stragglers, warmer and brighter than the metal-poor main-sequence turnoff (as indicated in **Figure 5**). Special evolutionary explanations must account for their anomalous HR diagram location. The *n*-capture abundance distributions of Ba-rich blue metal-poor stars mimic those of the cooler CH giants (e.g., figures 7 and 8 of Sneden, Preston & Cowan 2003).

Blue metal-poor stars and cool luminous CH giants each present unique challenges in *s*-process studies. In **Figure 8** we display the spectra near the Pb I 4057 Å-line of the CH giant HD 196944 (Van Eck et al. 2001) and the blue metal-poor star CS 29497-030. The metallicities of the two stars are almost identical, so the line strength differences of Fe-peak elements reflect the contrast in atmospheric parameters: The cool giant HD 196944 naturally has stronger line absorption. The atmospheric parameter effect is even more apparent in the CH features. The carbon abundance of CS 29497-030 ([C/Fe] ≃ +2.3, Ivans et al. 2005) is far larger than that of HD 196944 ([C/Fe] ≃ +1.3, Aoki et al. 2002b), yet the CH absorption in this spectral region is negligible in CS 29497-030. This makes derivation of the Pb abundance for CS 29497-030 much easier than for HD 196944, because CH is a major contaminant of the Pb I line. On the other hand, the physical state difference between the two stars creates severe difficulty in detection of

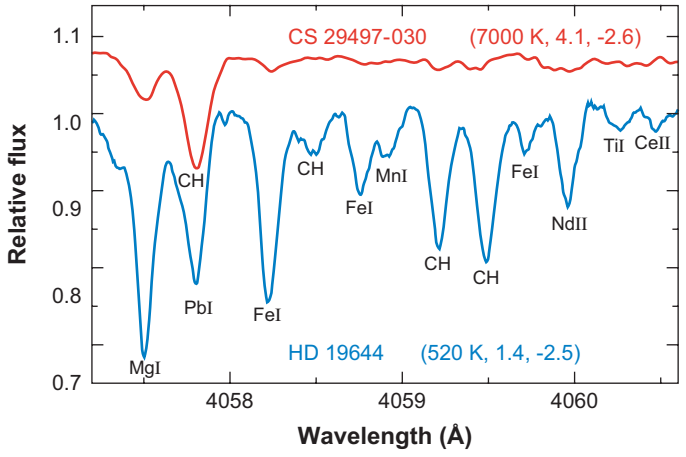

Figure 8

Observed spectra of C- and *s*-process-rich metal-poor stars HD 196944 (Van Eck et al. 2001) and CS 29497-030 (Ivans et al. 2005) near the Pb I line at 4058.8 Å. The derived atmospheric parameters ($T_{\rm eff}$, log *g*, [Fe/H]) for each star are quoted in the figure legend. The wavelength range of this plot has been chosen to match the HD 196944 Pb discovery spectrum (figure 1 of Van Eck et al.). The data shown here for that star are from S. Van Eck (private communication), smoothed to match the instrumental wavelength resolution of the CS 29497-030 spectrum. The Pb I line is blended with CH, but that contamination is extremely small in CS 29497-030 and a minority contribution to the feature in HD 196944 (see the synthetic spectrum match in the Van Eck et al. figure).

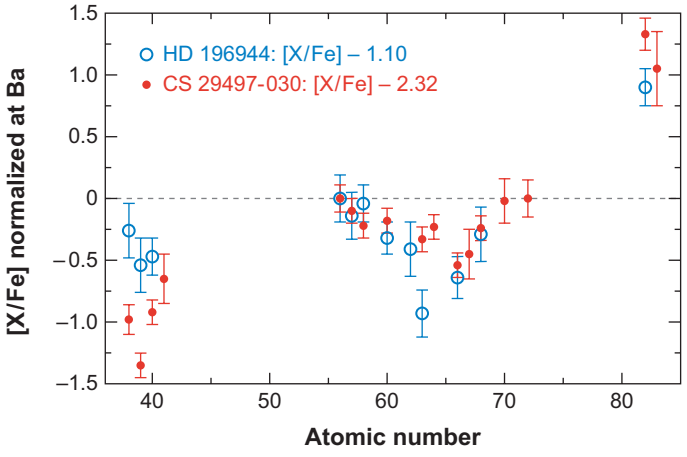

Figure 9

Observed abundance distributions of the Pb-rich stars HD 196944 and CS 29497-030, normalized to [Ba/Fe] ≡ 0.0. The actual [Ba/Fe] values of the two stars are noted in the figure legend. For CS 29497-030 the abundances are from Ivans et al. (2005), and for HD 196944 they are straight means of those reported by Van Eck et al. (2001) and Aoki et al. (2002c).

most *n*-capture spectral features in CS 29497-030, e.g., the very weak Nd II 4059.9 Å-line and nondetected Ce II 4060.5 Å-line that are easily seen in the HD 196944 spectrum.

In **Figure 9**, we compare the *n*-capture-element abundance distributions of these two Pb-rich stars. The overabundances of the *n*-capture elements average about a factor of 10 larger in CS 29497-030 than in HD 196944, so we have normalized the two data sets by subtracting their [Ba/Fe] values, as indicated in the figure legend. The overall abundance patterns are very similar. The major difference appears to be one of abundance slope, [X/Fe] as a function of atomic number Z. Similar patterns are seen in nearly all low-metallicity *s*-rich stars (e.g., Aoki et al. 2002c, Lucatello et al. 2003, Jonsell et al. 2006, Preston et al. 2006).

Finally, a large majority of C- and *s*-rich stars are members of binary systems. At high metallicity, spectroscopic binaries dominate the "Ba II" stars (McClure, Fletcher & Nemec 1980; McClure & Woodsworth 1990), and the same is true of the brighter lower metallicity CH stars (McClure 1984), and the "subgiant CH stars" (McClure 1997). Binarity is also the rule at low metallicity. Lucatello et al. (2005) detected radial velocity variations in 60% of a sample of C- and *s*-rich stars and argued on statistical grounds (see also Cohen et al. 2006) that nearly all stars of this type must be binaries. Preston & Sneden (2000) found that the binary fraction among blue metal-poor stars is about 2/3, again larger than expected, although not all of these stars are *s*-rich. The binaries typically have long orbital periods, 10^2–10^3 days, so they are currently not interacting. However, they have typically lower eccentricities than do normal field binary systems of comparable periods (see figure 19 of Preston & Sneden 2000). Additionally, nearly all of these binaries are single-lined; the companion is not detected. These observational facts taken as a whole suggest that the C- and *s*-rich stars received their abundance anomalies through mass transfer from a more massive AGB companion that is now a compact object.

6. *r*-PROCESS ABUNDANCE IMPLICATIONS

Early studies of the *r*-rich star CS 22892-052 (Sneden et al. 1996) yielded abundances from Ba ($Z = 56$) through the third *r*-process peak in CS 22892-052 in remarkable agreement with the

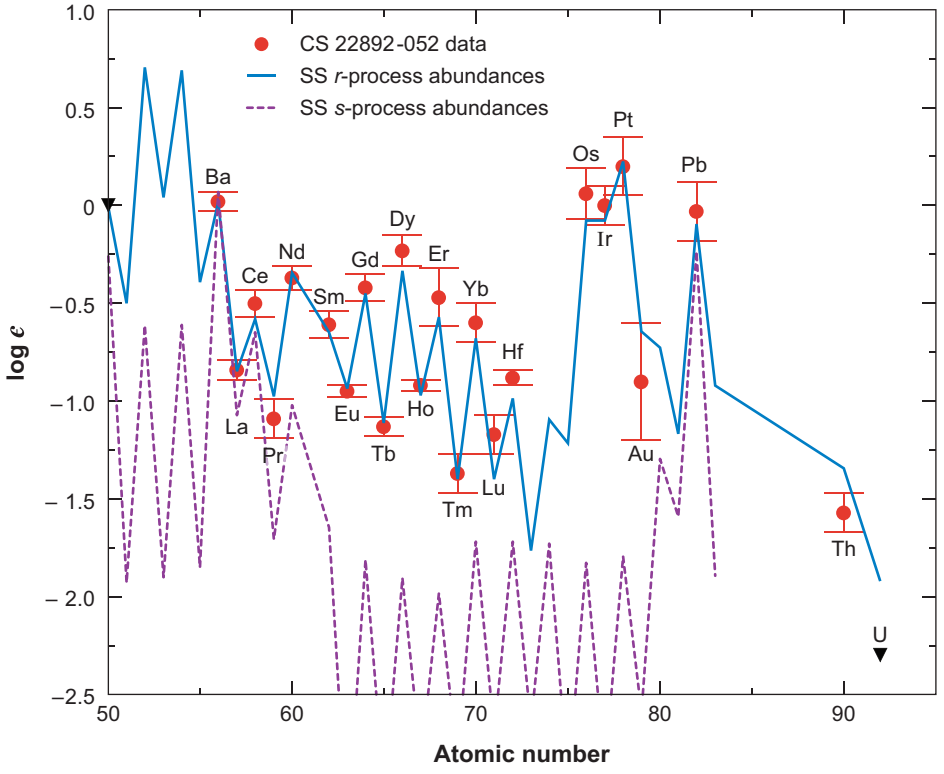

Figure 10

Comparison of CS 22892-052 Z ≥ 56 abundances with Solar-system *s*- (*purple dashed line*) and *r*-process-only (*solid blue line*) elemental abundance distributions. The CS 22892-052 data are from Sneden et al. (1996) with revised values for Nd (Den Hartog et al. 2003), Ho (Lawler, Sneden & Cowan 2004), Gd (Den Hartog et al. 2006), Sm (Lawler et al. 2006), and Hf (Lawler et al. 2007). The Solar-system curves are from Simmerer et al. (2004), as updated by Cowan et al. (2006). These curves have been normalized as follows: the *s*-process-only curve (*purple dashed line*) to the CS 22892-052 Ba abundance and the *r*-process-only (*blue solid line*) to the CS 22892-052 Eu abundance.

relative Solar-system *r*-element abundance distribution scaled to the overall rare-earth abundance level in this star. More recent work (Sneden et al. 2003), utilizing updated experimental atomic data to determine more accurate abundances, has confirmed this agreement. We illustrate this in **Figure 10**, where we compare the observed abundances for Ba and heavier elements in CS 22892-052 with *s*-process-only and *r*-process-only Solar-system elemental abundances. In both cases, these elemental curves have been obtained as described above, based upon elemental and isotopic abundance data in the classical model (Simmerer et al. 2004, Cowan et al. 2006). The *s*-process curve clearly does not fit the rest of the abundance data. It is obvious that the Solar-system *r*-process curve provides an excellent fit to all of the abundance data for the heaviest stable elements.

Although CS 22892-052 is very strongly enriched in *r*-process material, it was not clear at first whether this star might be somehow anomalous. But extensive observations of other *r*-rich stars have confirmed the same scaled Solar-system abundance pattern for elements with Z ≥ 56 (see, e.g., Westin et al. 2000, Cowan et al. 2002, Hill et al. 2002, Johnson 2002, Johnson & Bolte 2002b, Honda et al. 2004, Barklem et al. 2005, Ivans et al. 2006, Frebel et al. 2007). We present an updated compilation of the abundance data for these six *r*-rich stars in **Table 2**. In several cases

Table 2 Stellar abundance data for neutron-capture elements in *r*-process-rich stars

Element	Z	HD 221170[1] log ε	HD 115444[2] log ε	CB 22892-052[3] log ε	HE 1523-0901[4] log ε	BD 17 3248[5] log ε	CS 31082-001[6] log ε
Ga	31	0.59	–	–	–	–	–
Ge	32	–	–0.05	–	–	0.5	–
Rb	37	0.71	–	–	–	–	–
Sr	38	0.85	0.23	0.47	–	1.1	0.72
Y	39	−0.12	−0.82	−0.42	–	0.04	−0.23
Zr	40	0.66	−0.02	0.32	–	0.76	0.43
Nb	41	−0.17	–	−0.8	–	−0.18	−0.55
Mo	42	0.03	–	−0.4	–	–	–
Ru	44	0.33	–	0.08	–	–	0.36
Rh	45	−0.35	–	−0.55	–	–	−0.42
Pd	46	−0.03	–	−0.29	–	0.24	−0.05
Ag	47	−0.50	−1.25	−0.88	–	−0.28	−0.81
Ba	56	0.20	−0.68	0.02	0.28	0.44	0.4
La	57	−0.73	−1.44	−0.84	−0.63	−0.42	−0.62
Ce	58	−0.41	−1.1	−0.5	−0.25	−0.18	−0.31
Pr	59	−1.08	−1.82	−1.09	−0.75	−0.71	−0.86
Nd	60	−0.35	−0.93	−0.37	−0.02	−0.08	−0.13
Sm	62	−0.66	−1.26	−0.61	−0.38	−0.34	−0.51
Eu	63	−0.86	−1.64	−0.95	−0.62	−0.67	−0.72
Gd	64	−0.42	−1.08	−0.42	−0.17	−0.14	−0.27
Tb	65	−1.34	–	−1.13	–	−0.91	−1.26
Dy	66	−0.38	−1.01	−0.23	0.02	−0.03	−0.21
Ho	67	−0.97	−1.61	−0.92	–	−0.7	–
Er	68	−0.48	−1.21	−0.47	−0.29	−0.2	−0.27
Tm	69	−1.40	−1.79	−1.37	−1.13	−1.07	−1.24
Yb	70	−0.51	−1.4	−0.6	–	–	–
Lu	71	–	–	−1.17	–	–	–
Hf	72	−0.84	−1.51	−0.88	−0.73	−0.57	−0.72
Os	76	0.22	−0.55	0.06	0.18	0.45	0.43
Ir	77	0.02	–	0	0.24	0.3	0.2
Pt	78	–	−0.3	0.2	–	0.53	–
Au	79	–	–	−0.9	–	–	–
Pb	82	−0.09	−0.4	−0.03	–	–	–
Th	90	−1.46	−2.23	−1.57	−1.2	−1.18	−0.98
U	92	–	–	–	−2.06	−2	−1.92

[1]Ivans et al. (2006), with elemental updates from Lawler et al. (2007).
[2]Westin et al. (2000), with elemental updates provided by Den Hartog et al. (2003, 2006) and Lawler et al. (2004, 2006, 2007).
[3]Sneden et al. (2003), with elemental updates provided by Den Hartog et al. (2003, 2006), and Lawler et al. (2004, 2006, 2007).
[4]Frebel et al. (2007).
[5]Cowan et al. (2002), with elemental updates provided by Den Hartog et al. (2003, 2005, 2006) and Lawler et al. (2004, 2006, 2007).
[6]Hill et al. (2002), with elemental updates from Lawler et al. (2007).

the original abundance data sets have been revised based on new, more precise atomic data (from the sources given in the **Figure 10** caption).

We illustrate the concordance of the *r*-process abundance distributions in **Figure 11*a***, showing stellar abundances for six *r*-rich stars (vertically shifted for display purposes) compared with scaled Solar-system *r*-process-only abundances (*solid blue lines*). In **Figure 11*b*,*c***, we show individual relative offsets (Δ log ε) for the stars and their means with respect to the Solar-system *r*-only predictions from Simmerer et al. (2004) and the Arlandini et al. (1999) "stellar model," respectively. It is clear from the Figure that the stable (relative) elemental abundances for $Z \geq 56$ are in agreement for all six stars, and they follow closely the scaled Solar-system *r*-only curve. The root mean square offset of these elements in log ε is 0.10 for the comparison with the Simmerer et al. (2004) predictions. This value is consistent with zero, given the combined uncertainties in stellar and Solar-system abundances. This comparison was repeated for the stellar model of Arlandini et al. (**Figure 11*c***) with negligible difference to the outcome, confirming the consistency of Solar-system *r*-process abundance predictions. This extremely close agreement argues for the robust nature of the *r*-process, operating in much the same manner over the lifetime of the Galaxy.

Four of the six *r*-rich stars of **Figure 11** have very low metallicities, [Fe/H] ~ -3, implying that vigorous *r*-process production occurred at very early Galactic epochs. This process quickly began populating the heavier end of the Periodic Table. Assuming a relatively small time interval between the formation of the Galaxy and appearance of stars with [Fe/H] ~ -3, *r*-process synthesis sites must have been short-lived and rapidly evolving. This supports the idea that the first stars, progenitors of the observed halo stars, were likely massive and evolved quickly (Depagne et al. 2002; Qian & Wasserburg 2002; Qian, Sargent & Wasserburg 2002). Those objects needed to synthesize, eject, and mix the *r*-process elements into the halo interstellar medium (ISM) prior to the formation of the extreme *r*-rich stars. This points to a well-confined set of astrophysical and nuclear conditions that are responsible for *r*-process nucleosynthesis and suggests a relatively narrow range of masses for the astrophysical sites—presumably supernovae. Intriguingly, the robust nature of the abundance pattern in these halo stars, born perhaps before the Galaxy was fully formed, suggests a possibly more widespread agreement or relative consistency among our Galaxy and others.

The abundance comparisons of **Figure 11** can be turned around: The abundances in the *r*-rich stars can be used to predict the Solar-system *r*-only values. This has been done recently for several elements, including Gd (Den Hartog et al. 2006) and Hf (Lawler et al. 2007). In **Figure 12**, taken from Lawler et al., we form *s*-/*r*-process indicators with absolute abundance ratios log ε (La/Eu) for 10 well-known *r*-rich stars and plot these as a function of metallicity. The virtue of using La instead of the traditional Ba in this correlation lies in its often greater abundance reliability. La has only one isotope, and La II presents a larger number of less saturated absorption features than does Ba II; see the discussion in Simmerer et al. (2004). We also show dotted lines in the **Figure 12*a*** to indicate the range of published predictions for this ratio under *r*-process synthesis conditions. The average abundance value for La/Eu for these stars lies only slightly above the largest such predicted value. Then in **Figure 12*b***, the abundance ratios log ε (Hf/Eu) for these stars are displayed. The dotted line in **Figure 12*b*** indicates the current predicted *r*-only ratio. The solid line is the average ratios of the ten stars, which clearly falls above the current predicted Solar-system value. Lawler et al. (2007) conclude that there may be a somewhat larger contribution from the *r*-process to the production of Hf (and La) in Solar-system material than previously thought.

This process can be expanded to include other elements and to offer an additional method of deconvolving the Solar-system abundances. We list in **Table 3** some preliminary suggested values based on this technique. This exercise was only attempted for the stable elements from Ba to Pb. We have averaged the stellar data to predict the abundance offsets with respect to the current

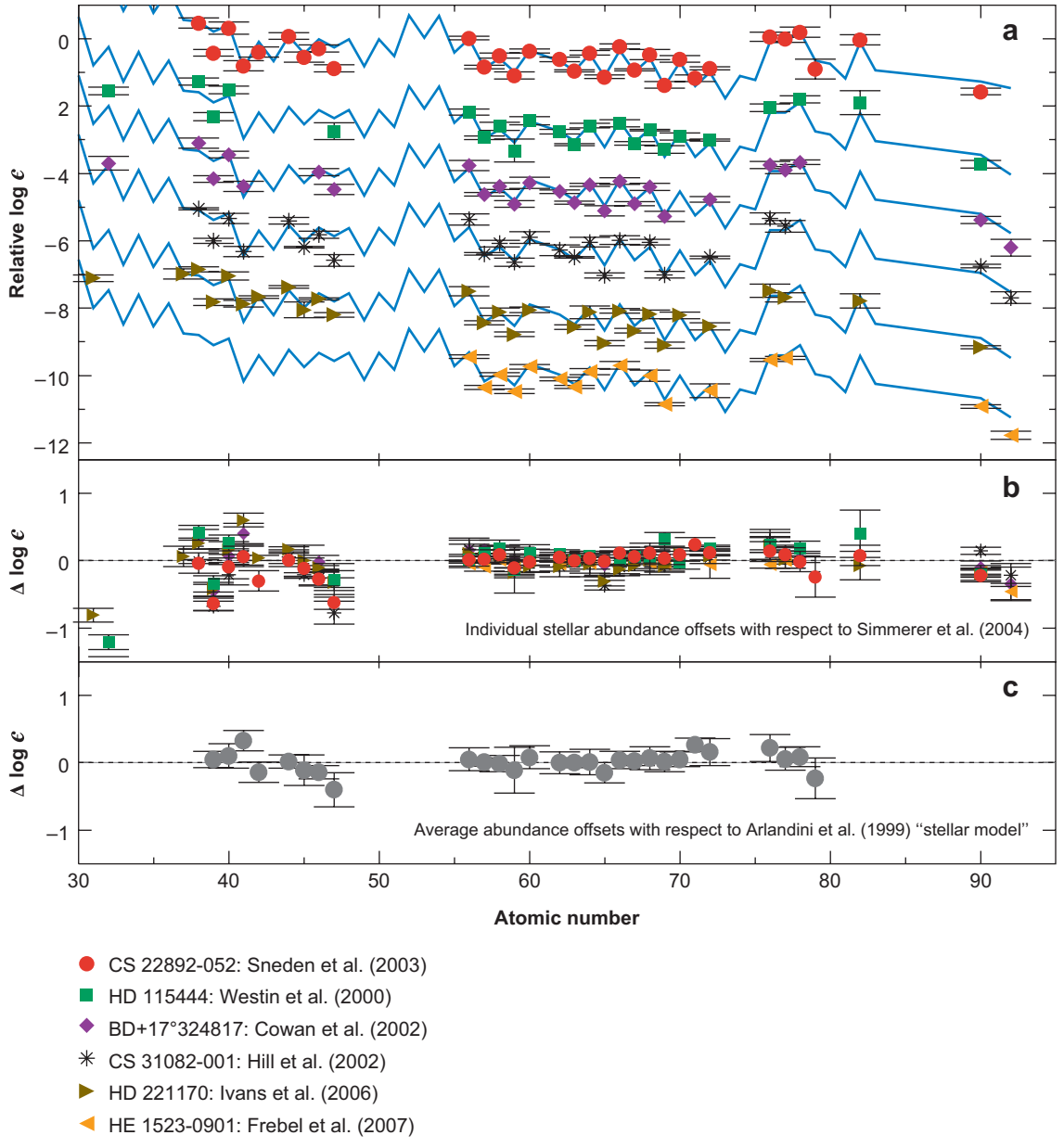

Figure 11

(*a*) Comparisons of *n*-capture abundances in six *r*-process-rich Galactic halo stars with the Solar-system *r*-only abundance distribution. The abundance data of all stars except CS 22892-052 have been vertically displaced downward for display purposes. The solid light blue lines are the scaled *r*-only Solar-system elemental abundance curves (Simmerer et al. 2004, Cowan et al. 2006), normalized to the Eu abundance of each star. (*b*) Difference plot showing the individual elemental abundance offsets; abundance differences are normalized to zero at Eu (see **Table 1** and **Table 2**) for each of the six stars with respect to the Solar-system *r*-process-only abundances. Zero offset is indicated by the dashed horizontal line. Symbols for the stars are the same as in panel *a*. (*c*) Average stellar abundance offsets. For individual stars all elemental abundances were first scaled to their Eu values, then averaged for all six stars, and finally compared to the Solar-system *r*-only distribution.

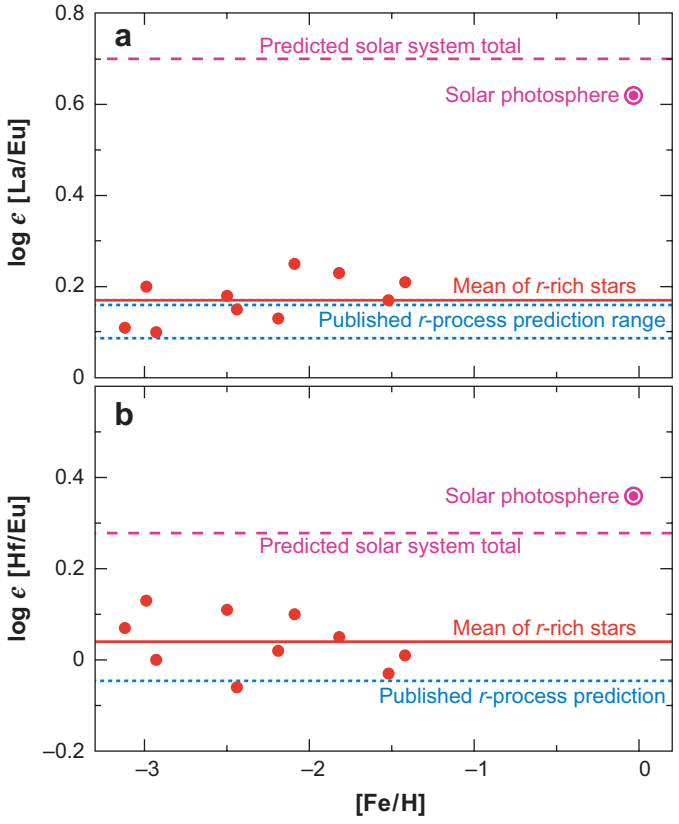

Figure 12

Abundance comparisons log ε [La/Eu] (*a*) and log ε [Hf/Eu] (*b*) versus metallicity, [Fe/H], for a group of 10 metal-poor, *r*-process-rich stars after Lawler et al. 2007. The red solid line is the mean ratio of the 10 halo stars, the magenta dashed line is the Solar-system total abundance, and the dotted blue lines indicate the predicted Solar-system *r*-process-only values for these ratios.

published Solar *r*-only value. Columns 1 and 2 of **Table 3** list the element name and Z value. In column 3 we show the relative average offsets. These have been obtained by first assuming that all of the Eu abundances agree completely with the Solar-system *r*-only value. Scaling the other stellar abundances with respect to Eu, the average offset, Δ, with respect to the Solar-system *r*-value for each element is then shown; by definition $\Delta = 0$ for Eu. We list in column 4 the elemental Solar-system *r*-only value, N_r [in meteoritic units of $N(\mathrm{Si}) = 10^6$], and in column 5 we list this same value in spectroscopic log ε units from Simmerer et al. (2004). The last two columns list our predicted Solar-system values for N_r and log $\varepsilon_{SSr,\,predicted}$ obtained by the addition of the offsets, Δ, to the current Solar-system published value of Simmerer et al. This same exercise was also done employing the Arlandini et al. (1999) stellar *s*-/*r*-process deconvolutions, with very similar results.

We caution that there are uncertainties in all of these abundance determinations including the initial Solar values, the *s*- and *r*-process breakdowns, and the average stellar abundance offsets. The predicted values should be viewed only as suggestive. In some cases, for example Er and Pr, the relatively large offsets are likely caused by a lack of precise atomic experimental data; efforts are underway to obtain such data. In the case of gold, with only one stellar detection with large errors bars, the average offset is not meaningful. However, in cases where newly determined and more precise

Table 3 Stellar-based Solar-system abundance predictions with respect to Simmerer et al. (2004)

Element	Z	Δ^1	$N_{r,SS}{}^2$	$\log(\varepsilon)_{r,SS}{}^3$	$N_{r,\ predicted\ SS}{}^4$	$\log(\varepsilon)_{r,\ predicted\ SS}{}^5$
Ga	31	−0.81	16.29	2.75	–	–
Ge	32	−1.42	56.23	3.29	–	–
Rb	37	0.06	2.89	2.00	–	–
Sr	38	0.19	2.55	1.95	–	–
Y	39	−0.51	1.31	1.66	–	–
Zr	40	0.04	2.04	1.85	–	–
Nb	41	0.29	0.11	0.58	–	–
Mo	42	−0.13	0.64	1.34	–	–
Ru	44	0.08	0.94	1.51	–	–
Rh	45	−0.10	0.29	1.00	–	–
Pd	46	−0.16	0.77	1.43	–	–
Ag	47	−0.46	0.43	1.18	–	–
Ba	56	0.07	0.81	1.45	0.94	1.51
La	57	0.04	0.11	0.58	0.12	0.62
Ce	58	0.16	0.20	0.85	0.30	1.01
Pr	59	−0.10	0.08	0.45	0.06	0.35
Nd	60	0.00	0.35	1.09	0.36	1.09
Sm	62	0.00	0.17	0.78	0.17	0.78
Eu	63	0.00	0.09	0.49	0.09	0.49
Gd	64	0.01	0.28	0.98	0.28	0.99
Tb	65	−0.18	0.06	0.32	0.04	0.13
Dy	66	0.00	0.36	1.10	0.36	1.10
Ho	67	0.01	0.08	0.46	0.09	0.47
Er	68	0.06	0.21	0.86	0.24	0.92
Tm	69	0.04	0.03	0.03	0.03	0.07
Yb	70	0.06	0.16	0.75	0.19	0.81
Lu	71	0.24	0.03	0.03	0.05	0.27
Hf	72	0.09	0.08	0.44	0.10	0.53
Os	76	0.18	0.65	1.35	0.99	1.54
Ir	77	0.06	0.65	1.35	0.74	1.41
Pt	78	0.07	1.30	1.65	1.53	1.72
Au	79	−0.24	0.18	0.79	0.10	0.54
Pb	82	0.14	0.62	1.33	0.85	1.47
Th	90	−0.12	0.04	0.09	–	–
U	92	−0.34	0.01	−0.49	–	–

[1]Average stellar abundance offsets with abundance differences normalized to zero at Eu, with respect to the SS *r*-process-only elemental abundance predictions.
[2]Solar-system *r*-process abundances with Si $= 10^6$.
[3]Solar-system *r*-process abundances in log ε units.
[4]Solar-system *r*-process abundance predictions based upon average stellar values with Si $= 10^6$.
[5]Solar-system *r*-process abundance predictions based upon average stellar values in log ε units.

stellar elemental abundance values are available, for example Hf described above, and where there is a relatively large average stellar offset (in this case, of 0.09), this might suggest a slight modification in the Solar-system *r*-process-only elemental value, as listed in the last columns of **Table 3**.

6.1. Isotopic Abundances

Additional evidence of the earliest Galactic *n*-capture nucleosynthesis can be obtained by isotopic abundance determinations. These are more difficult to obtain than elemental values because for most atomic transitions the wavelength displacements of individual isotopes are small compared to the thermal and turbulent broadening of the lines. A few exceptions exist, mainly among rare-earth elements.

The most extreme example is the *r*-process element Eu, which has naturally occurring isotopes ^{151}Eu and ^{153}Eu. Prominent Eu II lines have complex, very broad hyperfine and isotopic substructure, permitting accurate isotopic fractions to be estimated. Sneden et al. (2002), Aoki et al. (2003a) and Roederer et al. (2008) have found $f_{151} \equiv N(^{151}\mathrm{Eu})/N(\mathrm{Eu}) \simeq 0.5 \pm 0.1$ in several *r*-rich halo stars. Their results are in excellent agreement with the precise Eu meteoritic ratio of $f_{151} = 0.478$ (e.g., Lodders 2003), as well as the Solar photospheric ratio 0.50 ± 0.07 (Hauge 1972, Lawler et al. 2001), deduced from the same transitions that are used for *r*-rich stars. Aoki et al. (2003b) showed that two *s*-rich stars have $f_{151} \simeq 0.57$, in good agreement with *s*-process model predictions. In **Figure 13*d***, we summarize the Eu isotopic fraction measurements in low-metallicity stars. The difference between mean f_{151} values for *s*- and *r*-rich stars is suggestive, but determination of this fraction in larger samples of both types of stars would be welcome.

The first attempt at isotopic abundance assessment in metal-poor stars was for the much more challenging case of Ba. This element has five naturally occurring isotopes. The wavelength displacements of isotopic subcomponents are extremely small for all observable Ba II lines, but the odd-Z ^{135}Ba and ^{137}Ba have hyperfine substructures that produce a potentially detectable spread in the profile of the strong resonance line at 4554.0 Å. The *r*-process yields a larger fractional contribution to the elemental Ba abundance from the odd-Z isotopes than does the *s*-process. Therefore, careful analyses of the 4554 Å line to determine the odd-Z isotopic fraction, $f_{\mathrm{odd}} \equiv [N(^{135}\mathrm{Ba}) + N(^{137}\mathrm{Ba})]/N(\mathrm{Ba})$ can yield estimates of the *r*- and *s*-process contributions to a star's *n*-capture material. An initial attempt by Magain (1995) to detect an *r*-process component to the Ba abundance of the metal-poor ([Fe/H] ~ -2.4) subgiant HD 140283 produced a null result, but a reassessment by Lambert & Allende Prieto (2002) yielded $f_{odd}^{obs} = 0.30 \pm 0.21$. This value is marginally consistent with both a Solar-system *r*-only isotopic mix ($f_{odd}^{r} = 0.50 \pm 0.2$, Section 3.1 of Kratz et al. 2007) and with an *s*-only mix ($f_{odd}^{s} = 0.11 \pm 0.02$), as we visually show in **Figure 13*a***. However, uncertainties in both values are too large to make definitive statements on this issue. Assessments of f_{odd} for Ba in individual very metal-poor stars are likely to remain difficult because profile differences between *r*-process and *s*-process isotopic mixes compete with several other stellar atmospheric broadening effects for the 4554-Å line. As a final comment, Mashonkina & Zhao (2006) have estimated f_{odd} values for 25 thick- and thin-disk stars with $+0.3 >$ [Fe/H] $- 1.4$. This domain is much more metal rich than that considered in this review. However, Mashonkina & Zhao (2006) do demonstrate either an average increasing *r*-process, or decreasing *s*-process, contribution to Ba production (or some combination of these effects) as overall metallicity decreases; see their figure 6. Recent attempts have been made to explore isotopic abundance fractions of the rare-earth elements neodymium ($Z = 60$) and samarium ($Z = 62$). Lundqvist, Wahlgren & Hill (2007) explored Sm II line profiles in the *r*-rich star CS 31082-001 (Hill et al. 2002), concluding that they are suggestive of *r*-process dominance in the Sm isotopic mix. Roederer et al. (2008) then estimated the *r*-/*s*-process-sensitive isotopic fraction

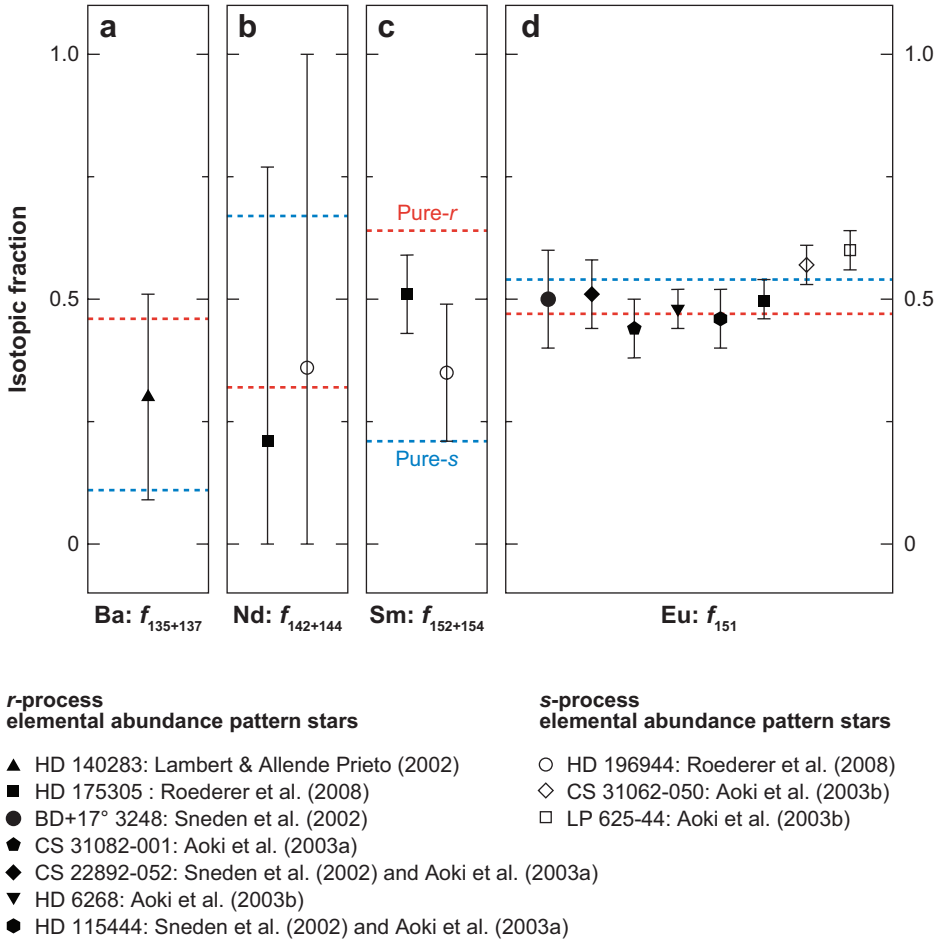

Figure 13

The isotopic fractions of Ba, Nd, Sm, and Eu as measured quantitatively in 10 metal-poor stars, after Roederer et al. 2008. The isotopic fraction (f_{iso}) is indicated for each species. The dashed red and blue lines in each panel represent the pure-*r*- and pure-*s*-process predictions, respectively, given by Arlandini et al. (1999).

$f_{152+154} = \{N(^{152}\text{Sm}) + N(^{154}\text{Sm})\}/N(\text{Sm})$ based on the classical model (see **Table 1**) and the stellar model from Arlandini et al. (1999) in two metal-poor stars with contrasting *n*-capture enrichment histories. The predicted fractions are $f_{152+154}^{r-only} = 0.64$ and $f_{152+154}^{s-only} = 0.21$. **Figure 13*c*** shows these predictions and the derived $f_{152+154}$ values for the two stars. As with Eu, the differences between the fractions are consistent with the elemental assignments of *r*-rich or *s*-rich to these stars, and again the observational situation is in need of a larger sample. Roederer et al. also estimated the ratio $f_{142+144} = \{N(^{142}\text{Nd}) + N(^{144}\text{Nd})\}/N(\text{Nd})$ in the same stars with Sm isotopic values. Unfortunately, the Nd isotopic wavelength splits are simply too small for the lines that were available in that study, and very large error bars attend the $f_{142+144}$ estimates, as shown in **Figure 13*b***.

Taken as a group, the Ba, Nd, Sm, and Eu isotopic fractions of the handful of low-metallicity stars studied to date are consistent with the elemental abundances. More effort should be put into such studies, which eventually should allow a much fuller understanding of the nucleosynthetic origin of these elements in the early Galaxy.

6.2. Multiple *r*-Process Sites?

It is apparent in **Figure 11** that the abundances of *n*-capture elements below Ba in *r*-rich stars do not conform very well to the Solar-system *r*-only abundances. We remind the reader of the cautions on the number of abundances and their reliability that were given in Section 4. In particular, no abundances are available for elements between Ag and Ba for any *n*-capture-rich stars. Only upper limits on Sn ($Z = 50$) have been derived for CS 22892-052 (Sneden et al. 2003) and HD 221170 (Ivans et al. 2006). The lack of abundance information in this element domain is a significant roadblock to theoretical interpretation of the *r*-process at low metallicity. Nevertheless, the reported deviations of the lighter elements from the Solar-system *r*-only abundance curve may indicate that there are different sites for different mass ranges of *r*-process elements.

Based on meteoritic data, Wasserburg, Busso & Gallino (1996) first suggested that the abundances of the lighter radioactive isotopes (in particular ^{129}I) and heavier isotopes (^{182}Hf) demanded different timescales for production and thus suggested two distinct *r*-process sites. Qian & Wasserburg (2000, 2001, 2002) and Wasserburg & Qian (2000) proposed different (supernovae) frequencies and mass ranges for these separate sites: (*a*) H (high-frequency) events that are the main source of heavy ($A > 130$) *r*-process nuclei but not ^{129}I; and (*b*) L (low-frequency) events that are largely responsible for light ($A < 130$) *r*-process nuclei including ^{129}I. These now two separate processes are referred to as strong for the heavier *r*-process and weak for the lighter *r*-process.

Where the elemental separation occurs between these two processes is, however, not clear. Recent *r*-process modeling work by Kratz et al. (2007) argues that I is produced along with Ba in the *r*-process, and therefore the dividing line between the weak and main falls below ^{129}I. Others have argued that two separate sites might not be required to produce the separate mass ranges of the *n*-capture elements. Instead, they argue that different epochs or regions of the same core collapse supernova could be responsible (see, e.g., Cameron 2001, 2003). It is impossible to pursue this issue to a conclusion without elemental abundances of I, or of those elements nearby in mass number, in the metal-poor *r*-rich stars.

Further complicating the elemental production picture are the findings regarding the elements Sr-Y-Zr. As discussed above in Section 4, there is a large star-to-star scatter in the abundances of these elements with respect to those of the heavier ($Z > 55$) elements. This scatter increases at lower metallicities and shows anticorrelations with other abundance ratios. Galactic chemical evolution (GCE) models to study these observations were performed by Travaglio et al. (2004), who suggested that the observed trends of the abundances of Sr, Y, Zr, Ba, and Eu versus metallicity could be understood "in light of a multiplicity of stellar neutron-capture components." They argued that the observed ratios of Sr, Y, and Zr to Ba and Eu versus metallicity provide diagnostics of the types of processes that formed Sr-Y-Zr, and that those elements must have a different origin than heavier elements such as Ba and Eu. Travaglio et al. further found that they could not explain the total Sr, Y, and Zr abundances in metal-poor halo stars employing only the main and weak *s*-process and the *r*-process. Instead, they suggested that 8% of Solar Sr and 18% of Solar Y and Zr must come from another primary process, which they named the Light Element Primary Process (LEPP). Refined calculations by Montes et al. (2007), attempting to reproduce the abundances of the *r*-process-poor star HD 122563 (Honda et al. 2006) and a sample of very metal-poor stars with various degrees of *r*-process enhancement, lend support to the existence of such a LEPP. Montes et al. have suggested that the nonuniform pattern in the halo stars for the lighter *n*-capture elements can be explained by a combination of the *r*-process and the LEPP. Qian & Wasserburg (2007) have also used the abundance observations in HD 122563 and CS 22892-052 to refine the predictions of their phenomenological model. They are also able to reproduce the elemental abundance patterns in the metal-poor halo stars with such a two component model. At this point in time, however, it

is still not clear that multiple sites are required for *r*-process nucleosynthesis or what the sites for these various mass ranges of *n*-capture elements observed in the halo stars might be.

7. EARLY GALACTIC NUCLEOSYNTHESIS

7.1. Some Trends with Metallicity

Large-sample surveys of halo stars with large metallicity ranges are providing new clues about the nature and extent of *n*-capture nucleosynthesis in the early Galaxy. Abundance signatures of these elements can help to identify the parameters of the first stars—long since gone—and the sites for *r*- and *s*-process nucleosynthesis (Cowan & Sneden 2006). There are many ways to approach this issue. We begin in **Figure 14** by contrasting the abundance behavior as a function of metallicity of the α element Mg and the *n*-capture element Eu. Only large stellar samples are employed for these correlations; the literature sources are listed in the figure caption.

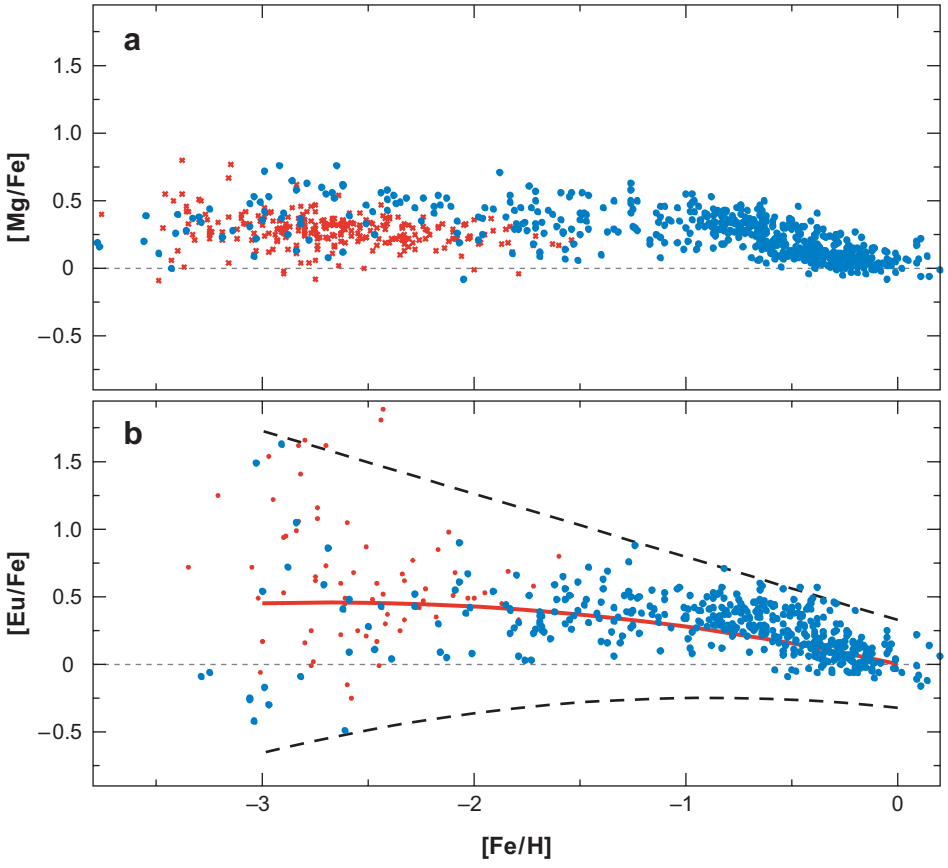

Figure 14

[Mg/Fe] and [Eu/Fe] abundances as a function of [Fe/H] metallicity for halo and disk stars. For this figure the data have been taken only from large-sample surveys: Fulbright (2000); Reddy et al. (2003); Cayrel et al. (2004); Cohen et al. (2004); Simmerer et al. (2004); Barklem et al. (2005, red points); Reddy, Lambert & Allende Prieto (2006); François et al. (2007). In both panels the dotted lines represent the Solar abundance ratios. In panel *b*, the solid red line is a least-square fit to the Eu data, and the two dashed black lines indicate the approximate extent of the Eu/Fe data (similar to Cowan & Thielemann 2004).

In **Figure 14*a*** we show the trend of [Mg/Fe] with [Fe/H]. This element has been chosen to represent the α group, because its abundance is based on relatively strong Mg I lines and thus has been reported for a large number of metal-poor stars. The characteristics of this correlation, which are thoroughly discussed in these survey papers and others, are: (*a*) There is very little scatter either at low- or high-metallicities, and (*b*) the overabundance [Mg/Fe] $\sim +0.3$ shows no significant drift with metallicity for stars with [Fe/H] < -1. The very small star-to-star scatter in particular has been emphasized by Cayrel et al. (2004) and Arnone et al. (2005). It is commonly thought that α-element production comes from massive stars (e.g., Timmes, Woosley & Weaver 1995; Woosley & Weaver 1995; Thielemann et al. 2000), and the data suggest that even at the lowest metallicities early in the Galaxy, there was significant Mg production. The downward trend of [Mg/Fe] to its Solar value is attributable to increasing Type I supernova iron production in the Galaxy. The relatively flat [Mg/Fe] ratio at low metallicity suggests that the types of stars that were synthesizing Fe in the Galactic halo were also synthesizing Mg. A few halo stars are known with [Mg/Fe] values substantially different from $\sim$+0.3 (e.g., McWilliam et al. 1995, Ryan, Norris, & Beers 1996, Aoki et al. 2007b, Ivans et al. 2003). This might indicate some degree of inhomogeneity in the Galaxy at that time, although the halo appears to have mixed in a relatively short timescale (e.g., Geisler et al. 2007).

In **Figure 14*b*** we plot [Eu/Fe] versus [Fe/H]. The dashed lines indicate (roughly) the extent of the data. The solid curved line is an approximate least-square fit to the data that significantly departs from [Eu/Fe] $= 0$ (*dotted line*) at lower metallicities. It is clear that, in contrast to the tightness of the [Mg/Fe] versus [Fe/H] correlation, there is significant [Eu/Fe] abundance scatter at low metallicities. For a specific example, [Eu/Fe] differs by about 2 dex in the very well-studied CS 22892-052 (e.g., Sneden et al. 2003) and HD 122563 (Honda et al. 2006). This large scatter was originally noted by Gilroy et al. (1988), and later expanded upon by, e.g., Burris et al. (2000) and Mishenina & Kovtyukh (2001), who argued that this was consistent with an early chemically unmixed Galaxy, with individual nucleosynthetic events (i.e., SNe) dominating and being widely scattered at those times. With increasing metallicities (and later times) this abundance scatter diminishes, presumably as the Galaxy becomes more chemically homogeneous.

These data further suggest that *r*-process production was rare in the early Galaxy—that only a few stars synthesized elements such as Eu, and that Mg and Fe production was not strongly coupled to *r*-process production. Different mass ranges for the sites for the α elements and the *r*-process elements are indicated. This interpretation is consistent with the scenario and analytic models proposed by Fields, Truran & Cowan (2002; but see also Wasserburg & Qian 2000 for a different interpretation). The downward slope of the [Eu/Fe] data with higher metallicities, similar to that of [Mg/Fe], is also due to increasing production of Fe from Type Ia SNe. Interestingly, this curve mimics models of *r*-process nucleosynthesis from lower-mass ($\approx$8–10 $M_\odot$ SNe; see, e.g., Mathews, Bazan & Cowan 1992; Wheeler, Cowan & Hillebrandt 1998; Ishimaru & Wanajo 1999; Raiteri et al. 1999; Travaglio, Galli & Burkert 2001; Cowan & Thielemann 2004).

Galactic evolution in *r*- and *s*-process production can be seen in **Figure 15**, which presents a large-sample correlation with metallicity of abundance ratios of La (a largely *s*-process element in Solar-system material) to Eu (an *r*-process element). A solid horizontal line in **Figure 15** represents the average log ε (La/Eu) value of the 10 *r*-rich stars that were considered earlier in **Figure 12**. Also illustrated are several horizontal lines drawn near log ε (La/Eu) $\simeq 0.1$ to indicate the range of recent predictions for this ratio in *r*-process synthesis conditions (which are consistent with the observations of very *r*-rich stars; see Section 6). The data of **Figure 15** show that the mean log ε (La/Eu) value grows with increasing metallicity, and significant Galactic *s*-process nucleosynthesis appears to occur at [Fe/H] $\gtrsim -2$. However, already at very low metallicities there are clear indications of the *s*-process (e.g., Simmerer et al. 2004). It may be, as noted above, that much of

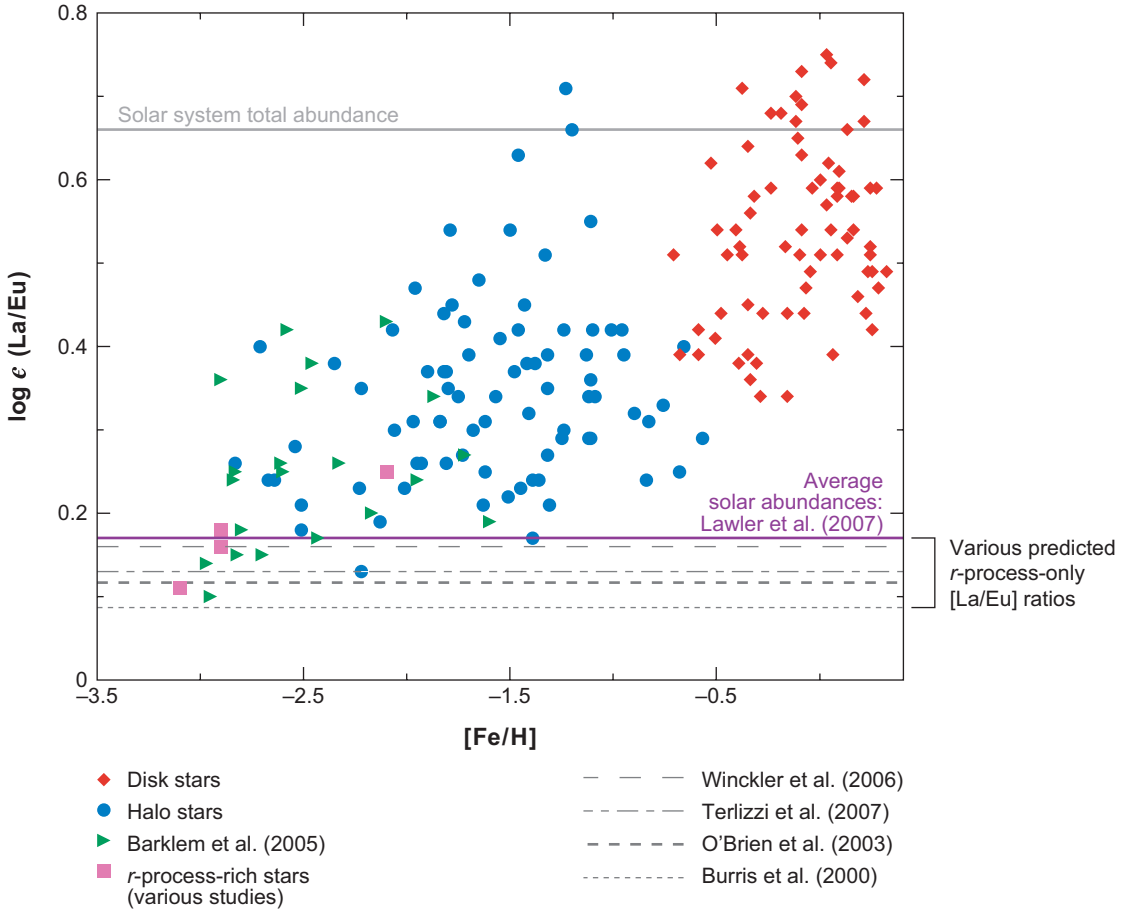

Figure 15

Abundance trends with respect to metallicity for the elemental ratio La/Eu in a large number of stars in our Galaxy (after Simmerer et al. 2004). The pink boxes are well-studied *r*-process-rich stars, including CS 22892-052, HD 115444, CS 31082-001, and BD+17°3248.

that early *s*-processing could be associated with binary mass transfer. Or perhaps sources other than low-mass stars could have made some small contributions at these low metallicities. The bulk of the Galactic *s*-processing, however, could not have occurred until a time equivalent to [Fe/H] $\gtrsim -2$, or after the evolution of low-mass single (or binary) stars, the main sites for the *s*-process. Identifying the exact metallicity, and ultimately the timescales for this onset, will provide further insight into the types and masses of stars that were responsible for *s*-process nucleosynthesis early in the Galaxy.

Finally, consider Ge ($Z = 32$), which is classified as an *n*-capture element. Only recently has much Ge abundance data become available (Cowan et al. 2005). These are illustrated in **Figure 16** for a sample of 11 Galactic halo stars. Surprisingly, the data indicate a tight correlation of Ge with Fe: [Ge/H] = [Fe/H] − 0.79; there is very little relationship between Ge and Eu abundances. This seems to indicate that the Ge production is tied for low-metallicity stars to the Fe production, i.e., that charged particle reactions are able to synthesize both of these elements. This has led to the suggestion of a new neutrino scattering process in supernovae that would produce some protons that could be captured on Fe-peak nuclei to synthesize Ge (Fröhlich et al. 2006). Although this explanation seems to fit the data at early times in the Galaxy, it would be expected that the

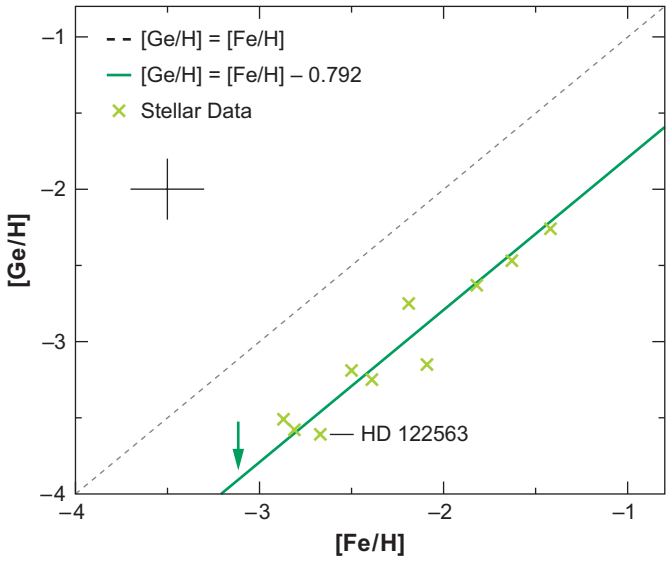

Figure 16

[Ge/H] abundances in a sample of 11 Galactic halo stars as a function of metallicity. The arrow denotes the upper limit for the CS 22892-052. The dashed line represents the Solar abundance ratio of these elements, [Ge/H] = [Fe/H], and the solid green line shows the derived correlation, [Ge/H] = [Fe/H] − 0.79, for all the stars, after Cowan et al. 2005.

appearance of major Galactic weak *s*-process contributions might change the shape of this curve with the addition of Ge and other very light *n*-capture elements. Unfortunately there are no current metal-rich stellar Ge data available.

Increasing evidence suggests that the abundance patterns of the very metal-poor stars in other nearby galaxies exhibit *s*- and *r*-process abundances similar to those of Galactic halo stars (Shetrone et al. 2003, Venn et al. 2004). This may have implications for the nature of the earliest (or first) stellar generations. There appear to be significant differences—particularly for the α elements—between the metal-rich Galactic stars and similar stars in nearby dwarf spheroidal/irregular galaxies (resulting from, for example, different star-formation rates), but those differences lessen as the metallicity decreases (Geisler et al. 2007). These abundance comparisons have implications for the formation of the Galactic halo and galaxy formation in general. The robust nature of the abundance patterns of the halo stars and the apparent widespread similarities in relative *n*-capture element abundance patterns for the very metal-poor stars, from galaxy to galaxy, seem to suggest that the synthesis processes (particularly the *r*-process) might have been operating in a somewhat consistent manner in the early Universe.

7.2. Nucleocosmochronometry

The earliest generations of (massive and short-lived) stars ejected *r*-process-rich material by SN explosions into the halo ISM, where it was gathered into the low-mass (thus long-lived) very metal-poor stars that we see today. This SN-synthesized material also contains radioactive elements, such as the long-lived uranium and thorium isotopes, produced solely in the *r*-process. The observed ratio of one of these radioactive elements to a stable *r*-process-dominated element can in principle be utilized to predict the time for the formation of these elements, very early in the history of the Galaxy, closely approximating the age of the Galaxy.

Originally proposed in a pioneering study by Butcher (1987) as a means of determining the age of the Universe, the technique initially concentrated on Th. That work suffered owing to (*a*) its application to higher metallicity Galactic disk stars (the single Th II line at 4019.1 Å used by Butcher and most subsequent studies is part of a complex blended spectral feature), and (*b*) the use of Nd as the comparison element (Nd has a substantial *s*-process component to its abundance in metal-rich stars). Substantial improvement was achieved by François, Spite & Spite (1993), who concentrated on metal-poor halo stars and used the more nearly pure *r*-process element Eu to contrast with Th. Today, with better understanding of the blending issues of the 4019 Å line, detection of other Th II lines in metal-poor, *r*-rich field halo stars (e.g., Cayrel et al. 2001, Johnson & Bolte 2001, Hill et al. 2002, Honda et al. 2004, Ivans et al. 2006, Frebel et al. 2007), the globular cluster M15 (Sneden et al. 2000b), and even a member of a nearby dwarf spheroidal galaxy (Aoki et al. 2007c), there have been a number of stellar Th/Eu cosmochronometeric age determinations (see, e.g., Sneden et al. 1996, 2000a, 2003; Cowan et al. 1997, 1999; Pfeiffer, Kratz & Thielemann 1997; Westin et al. 2000; Johnson & Bolte 2001; del Peloso et al. 2005, and references therein).

One of the strengths of this technique is that it is independent of chemical evolution and cosmological models. Instead, it relies upon determining the elemental radioactive abundances in the halo stars and knowing what the initial (production) ratio is in the astrophysical *r*-process site. The observed Th/Eu ratio has been found to be $\log \varepsilon\,(\mathrm{Th/Eu}) = -0.60$ ($\sigma = 0.05$) in HD 221170 [Ivans et al. 2006, a value very similar to that found for a number of other very metal-poor field stars including HD 115444 (−0.60, Westin et al. 2000), BD+17°3248 (−0.51, Cowan et al. 2002), CS 22892-052 (−0.62, Sneden et al. 2003), and HE 1523-0901 (−0.58, Frebel et al. 2007)]. This same abundance ratio for HD 221170 is also consistent with the average ratio found in two giant stars of the globular cluster M15: $\langle \log \varepsilon\,(\mathrm{Th/Eu}) \rangle = -0.62$ (Sneden et al. 2000b).

The chronometric age estimates depend sensitively on the initial values of Th/Eu predicted for the *r*-process. This in turn depends on the nuclear mass formulae and *r*-process models employed in making those determinations (see discussion in Schatz et al. 2002 and Cowan & Sneden 2004). Calculations of the *r*-process are designed to replicate the Solar-system isotopic and elemental abundance distributions. The same calculations that reproduce the stable Solar-system and stellar elemental abundances are then used to predict the radioactive abundances and thus the Th/Eu ratio (see further discussion in Kratz et al. 2004, 2007). Comparing predicted and observed Th/Eu abundances has led, in most cases, to consistent age determinations (e.g., CS 22892-052, HD 115444, and BD +17°3248) of 12–14 Gyr ±2–3 Gyr. The total derived age uncertainties combine both observational uncertainties and those associated with the initial production ratios (e.g., nuclear mass formulae, etc.). The calculated values of this production ratio vary widely (see Cowan, Thielemann & Truran 1991b); some recent determinations fall between 0.48 and 0.42 in an *r*-process site (Cowan et al. 1999, Sneden et al. 2003, Kratz et al. 2004).

There has been concern regarding use of the Th/Eu as a chronometer, principally owing to the large nuclear mass-number gap ($\delta A \simeq 80$) between Eu and Th (e.g., Goriely & Arnould 2001). A more ideal chronometer would be the ratio of Th/U, because both are made in the *r*-process and similar in atomic mass. Uranium has only been observed in a few stars, starting with its detection in CS 31082-001 (Cayrel et al. 2001). Th/U has been employed to determine the chronometric age of CS 31082-001 (12.5 ± 3 Gyr, Cayrel et al. 2001; 14 ± 2.4 Gyr, Hill et al. 2002; 15.5 ± 3.2 Gyr, Schatz et al. 2002; 14.1 ± 2.5 Gyr, Wanajo et al. 2002). However, in the case of CS 31082-001, the Th/Eu ratio gives an age inconsistent with Th/U and with the chronometric age estimates of other halo stars. This suggests that Th/Eu is not always a reliable chronometer. In fact the Th/Eu value in this star would imply an age less than that of the Solar-system! The large values of Th and U in this star (Hill et al. 2002) have been interpreted as being produced by an "actinide boost" that might, for example, be consistent with fission recycling (Schatz et al. 2002).

It is still not clear whether the large overabundances of Th and U in CS 31082-001 are singular features of this particular star or whether an entire class of actinide-boost stars exists. Another concern with this particular star is its lead content, which predominantly results from α decay of Th and U isotopes. Plez et al. (2004) have derived a Pb abundance that seems to be too low with respect to such high abundance values of radioactive elements Th and U (Kratz et al. 2004). Some reports of high Th/Eu abundance ratios in other stars (e.g., Yushchenko et al. 2005) have been revised significantly downward upon reanalysis with better stellar spectroscopic and atomic data (Ivans et al. 2006).

Very recently, uranium has been detected in HE 1523-0901 by Frebel et al. (2007), and in **Figure 17** we reproduce their comparison of the U II 3859.6 Å feature in this star and in CS 31082-001. Frebel et al. employ observed ratios of U/Th, U/Ir, Th/Eu, and Th/Os to measure the stellar age, finding that all chronometer pair ratios including Th/Eu yield relatively consistent

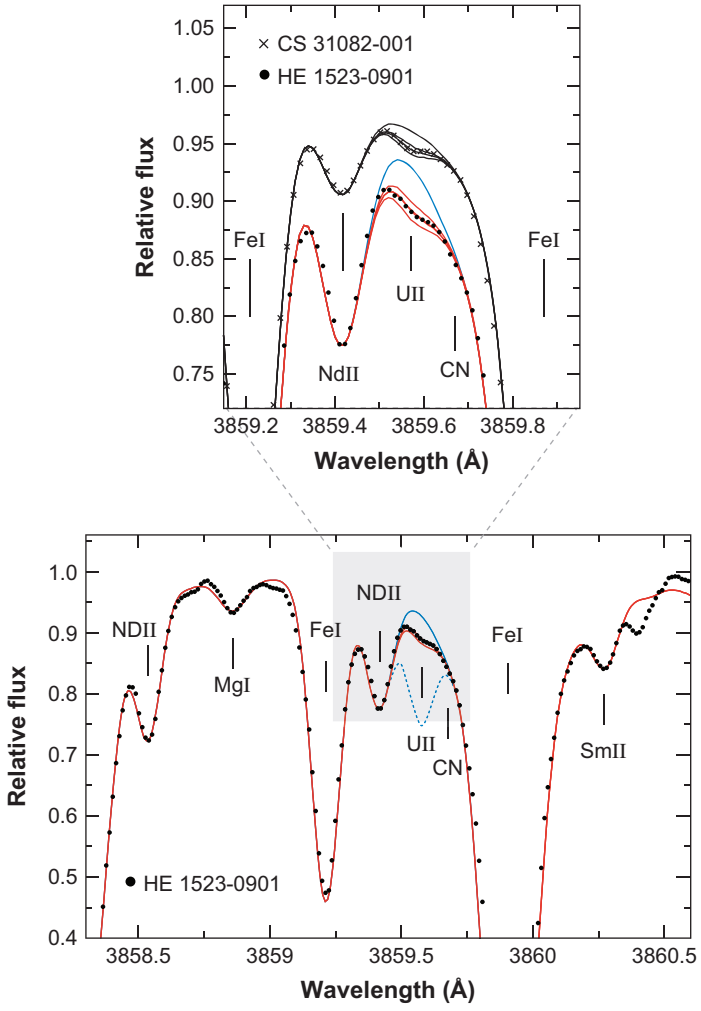

Figure 17

Uranium lines for CS 31082-001 and HE 1523-0901 from Frebel et al. 2007. Synthetic spectra are shown for no contribution from U II, for the best-fit implied U abundance, and ± 0.1 dex deviations from that fit.

ages. They derive a value of 13.2 ± 2.7 Gyr for HE 1523-0901. Finally, a tentative detection of U was reported for BD+17°3248 by Cowan et al. (2002), and the Th/U and Th/Eu ratios also give consistent ages for this star.

Although Th/U is a good choice for chronometer studies, the inherent weakness of U II lines and severe blending issues will likely limit the number of stars in which this chronometer pair can be employed. There may, however, be another possible choice. Recent *r*-process calculations by Kratz et al. (2007) that successfully reproduced the third (and most massive) *r*-process peak also indicate that *r*-process production of the element Hf (shown in Section 6 to correlate well with the *r*-process-element Eu) follows closely those of third-peak elements such as Pt. We illustrate this in **Figure 18**, taken from Kratz et al., where we plot the behavior of the abundances of this interpeak element compared with Pt, Eu, Th, and Pb. Thus, Hf, which is observable with ground-based telescopes (Lawler et al. 2007) and is near in nuclear mass number to the third *r*-process peak

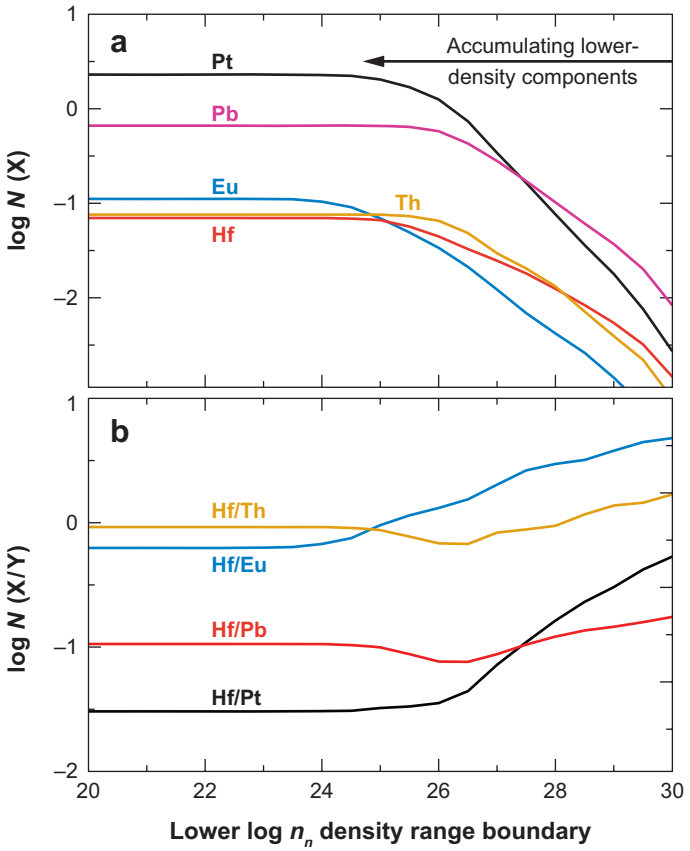

Figure 18

(*a*) The weighted abundance accumulations of each element are plotted. These are computed starting with the predicted abundances at the highest neutron density, log $n_n = 30$, and adding the abundances at successively lower values of log n_n. The abundances of particular elements "saturate" at their Solar-system *r*-process numbers, when the contributions of even smaller neutron density regimes cease to add to their abundances. (*b*) Abundance variations of selected ratios are plotted as a function of neutron number density (after Kratz et al. 2007).

elements, might also be employed in Th/Hf ratios as a possible new stellar age chronometer (see Kratz et al. 2007 for further discussion).

The average values obtained for the chronometric ages of the halo stars ($\simeq$12–14 Gyr) agree quite well with other age determinations. These include employing Th/U in meteorites, in conjunction with observations of halo stars and coupled with a chemical evolution model, to determine the age of the Galaxy ($14.5^{+2.8}_{-2.2}$ Gyr, Dauphas 2005). Other age estimates include those from the Wilkinson Microwave Anisotropy Probe, combined both with results from the Sloan Digital Sky Survey ($14.1^{+1.0}_{-1.9}$ Gyr; Tegmark et al. 2004), as well as with earlier cosmic microwave background (CMB) and large-scale structure data (13.7 ± 0.2 Gyr; Spergel et al. 2003); globular cluster results based upon main sequence turn-off ages ($12.5^{+3.5}_{-2.4}$ Gyr, Krauss & Chaboyer 2003; or $12.6^{+3.4}_{-2.2}$ with the inclusion of CMB data, Jimenez et al. 2003); and a white dwarf cooling curve age of 12.1 $\pm$ 0.9 Gyr for globular cluster M4 (NGC 6121; Hansen et al. 2004). Nucleocosmochronology offers promise as an independent dating technique. Further refinements and increasingly precise determinations ultimately will place stronger constraints on other cosmological age estimates and models.

8. *s*-PROCESS ABUNDANCE IMPLICATIONS

8.1. Asymptotic Giant Branch Stars and *s*-Process Nucleosynthesis

Theoretical studies have led to the identification of the *s*-process site in low- to intermediate-mass stars (i.e., $M \simeq 1.3 - 8\ M_{\odot}$) during the AGB phase (see reviews by Busso, Gallino & Wasserburg 1999; Busso et al. 2004). The major neutron source in AGB stars is provided by the primary-like $^{13}C(\alpha, n)^{16}O$ reaction occurring in the He-rich zone in radiative conditions (Straniero et al. 1997) during the interpulse phase. During a so-called third dredge-up (TDU) episode the H-rich convective envelope comes in contact with the inner He-rich and ^{12}C-rich zone (He intershell), while the H-shell is inactive. A small number of protons from the envelope are assumed to penetrate into the top layers of the He intershell (see discussion in Hollowell & Iben 1988). At H reignition, proton capture on the abundant ^{12}C gives rise to a tiny ^{13}C-pocket via the reaction chain $^{12}C(p, \gamma)\ ^{13}N(\beta^+\nu)\ ^{13}C$. This region is further compressed and heated, and at $T \approx 0.9 \times 10^8$ K neutrons are released by the ^{13}C neutron source before the development of the next convective thermal instability in the He shell. Thus, most of the *s*-process production occurs in the pocket where the neutron density is $\sim 10^7$ cm^{-3}. Note that the neutrons released in the pocket in principle do not depend on metallicity.

The amount of ^{13}C cannot be fixed from physical principles and so the efficiency of neutron production may vary from star to star. Rotational mixing, shear turbulence, gravitational waves, thermodynamical instability at the border between the upper H-rich convective envelope and the lower C-rich and He-rich radiative He intershell, or other physical mechanisms, based on specific hydrodynamical treatment, may affect the downflow of protons from the envelope. Arlandini et al. (1999) were able to reproduce the Solar-system main *s*-component predicted by the classical analysis using an "ad hoc" ^{13}C pocket for AGB models of half-Solar metallicity (the so-called standard ^{13}C pocket, hereafter ST). The main *s*-process component deduced from the AGB yields of half-Solar metallicity and the ST pocket case (Arlandini et al. 1999) of course represent a very first approximation to the true situation.

An effective maximum to the ^{13}C pocket naturally arises. If the amount of ^{13}C is more than about $2 \times$ ST then the higher abundance of protons diffused from the envelope results in preferential production of ^{14}N (a severe neutron poison) rather than ^{13}C. For near-Solar metallicities there is also an effective minimum choice of the ^{13}C pocket efficiency corresponding

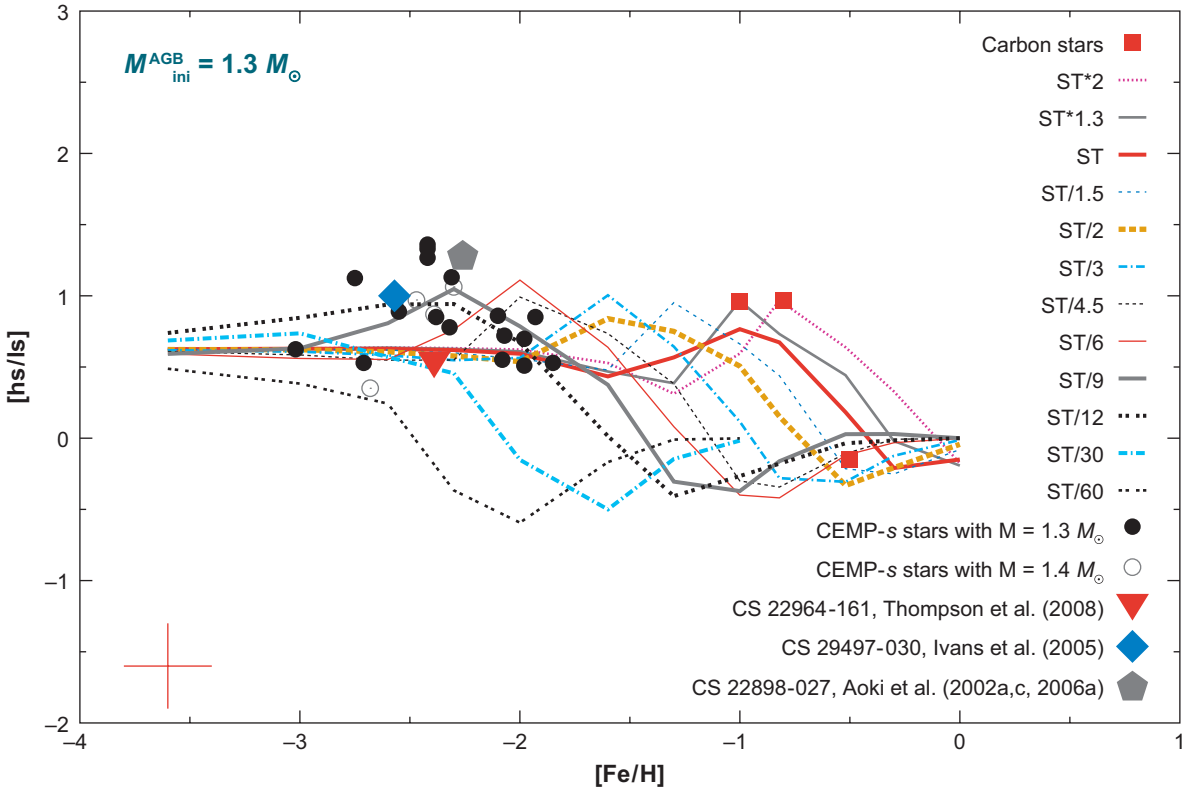

Figure 19

Theoretical predictions of [hs/ls] ("second" to "first" *s*-process peak elements) versus [Fe/H] for AGB stars of initial mass 1.3 $M_\odot$ and 1.4 $M_\odot$ for different ^{13}C pocket efficiencies, and observed values for CEMP-*s* stars, three metal-poor C(N) stars in the Local Group (de Laverny et al. 2006). The representative points of the CEMP-*s* stars reported are from Aoki et al. (2002a,c, 2006a, 2007a), Barbuy et al. (2005), Barklem et al. (2005), Cohen et al. (2003, 2006), Ivans et al. (2005), Johnson & Bolte (2002a, 2004), Jonsell et al. (2006), Lucatello et al. (2003), Preston & Sneden (2001), and Thompson et al. (2008).

to about the case of ST/12, below which the *s*-process distribution does not change anymore. This minimum value decreases substantially at halo metallicities, given the far lower abundance of the Fe seeds. In essence, the choice of the ^{13}C concentration in the pocket is left as a free parameter, in the range of the upper and lower limits specified above, to be calibrated by observational constraints (Busso et al. 2001, Abia et al. 2002, Gallino et al. 2005, Bisterzo et al. 2006a,b).

Varying [Fe/H] has a profound impact on the *s*-process isotope and elemental distribution. **Figure 19** shows [hs/ls], second/first *s*-process peak elements, versus [Fe/H] predictions for AGB stars of initial mass 1.3 $M_\odot$ and 1.4 $M_\odot$ and different ^{13}C pocket efficiencies. In this figure the ^{13}C pocket efficiency has been allowed to vary over a wide interval, as indicated by the labels, with the amount of ^{13}C nuclei in the pocket being multiplied or divided with respect to case ST by the indicated factors. The figure also contains representative abundance data for a sample of low-metallicity C(N) stars in the Local Group (literature sources are given in the figure caption), and CEMP-*s* stars for which an AGB initial mass has been assumed (see Section 8.2).

The [hs/ls] ratio is independent of whether an observed *s*-enhanced star is an intrinsic AGB (generating its *s*-process elements internally) or an extrinsic AGB (receiving these elements via binary mass transfer). For a given ^{13}C pocket efficiency, e.g., the ST choice, the number of neutrons captured per Fe seed nucleus increases linearly with decreasing metallicity. Consequently, the mean neutron exposure characterizing the *s*-process distribution also increases linearly with decreasing metallicity (Busso, Gallino & Wasserburg 1999). Starting from Solar, the [hs/ls] ratio first increases with decreasing [Fe/H]. As the metallicity further decreases, the [hs/ls] ratio reaches a maximum at [Fe/H] $= -1$ and then decreases. This behavior is due to the progressive buildup of the third *s*-peak at Pb, which becomes dominant over the ls and hs production at a metallicity of [Fe/H] $= -1$.

For a range of Galactic disk metallicities an acceptable fit to the main *s*-component can be obtained for a suitable ^{13}C pocket. For example, almost the same *s*-process distributions are produced for these cases: (*a*) [Fe/H] $= -0.3$ and ST; (*b*) [Fe/H] $= 0.0$ and ST $\times$ 2; and (*c*) [Fe/H] $= -0.6$ and ST/2. This relationship breaks down with decreasing metallicity, where the impact of Pb production becomes more and more pronounced. However, as long as the overall neutron exposure is capable of pushing the *s*-process beyond its second *s*-process peak, an almost flat *s*-process distribution is predicted by the rule $\sigma(A)Ns(A) \sim$ constant in the atomic mass region from Ba to ^{204}Pb. This result is independent of metallicity or the ^{13}C-pocket efficiency. Therefore, the *r*-process fractions of Solar abundances in this atomic mass region, deduced by the residual method, should be unaffected by the *s*-process analytical details. In conclusion, both the main and the strong *s*-components of *n*-capture isotopes result from many generations of AGB stars polluting the ISM prior to Solar-system formation.

8.2. The *s*-Process in Carbon-Enhanced Metal-Poor *s*-Process-Rich Stars

Nearly all CEMP-*s* stars are dwarfs or giants of low luminosities—much lower than true AGB stars. The *n*-capture elements seen in CEMP-*s* stars are the result of mass transfer from the winds of an AGB (now an undetected WD) primary companion. These abundances provide insight into the *s*-process and C yields generated by low-metallicity, low-mass stars at the earliest Galactic epochs. For various ^{13}C-pocket efficiencies at the end of the AGB phase and for AGB models of initial mass 1.5 $M_{\odot}$, large photospheric abundances are predicted for C, Na, and Mg and for all the *s*-process elements. The predicted ratio, for example, for [La/Eu] ~ 1. Lead shows the largest overall enhancement, but its abundance is very sensitive to the ^{13}C pocket efficiency. Decreasing from case ST down to case ST/30 produces a decrease of almost 2 dex in [Pb/Fe]. For the ST $\times$ 2 case the Pb envelope abundance is a hundred times larger than in the Sun! In contrast, the predicted [ls/Fe] and [hs/Fe] ratios are less sensitive to the adopted ^{13}C pocket efficiency. These tendencies can be ascribed to the primary-like ^{13}C neutron source impacting on so few Fe seeds. Most of the *s*-fluence builds up to Pb, after having left behind a sort of plateau, first in the ls and then in the hs abundances. This explains the similar [ls/Fe] and [hs/Fe] element ratios seen in many CEMP-*s* stars (Section 5). This is in contrast to the large scatter in the observed [Pb/hs] ratio seen in these stars, as illustrated in **Figure 20**.

The predicted [C/Fe] does not depend on the ^{13}C-pocket efficiency. Rather, it reflects the large mass fraction abundance $X(^{12}\text{C}) \sim 0.25$ in the He intershell at the quenching of a thermal instability, from partial 3α burning in the thermal pulse. A lower [C/Fe] value in the envelope might be conceivable in the case of the operation of the so-called cool bottom process (CBP) operating during the AGB phase (Nollett, Busso & Wasserburg 2003, Wasserburg, Busso & Gallino 2006), with a correspondingly important increase in [N/Fe]. In the AGB models the CBP has not been included and only a moderate [N/Fe] ~ 0.6 dex is predicted in the envelope, as a consequence of the first dredge up when the star ascends the Red Giant Branch. Note that the material mixed

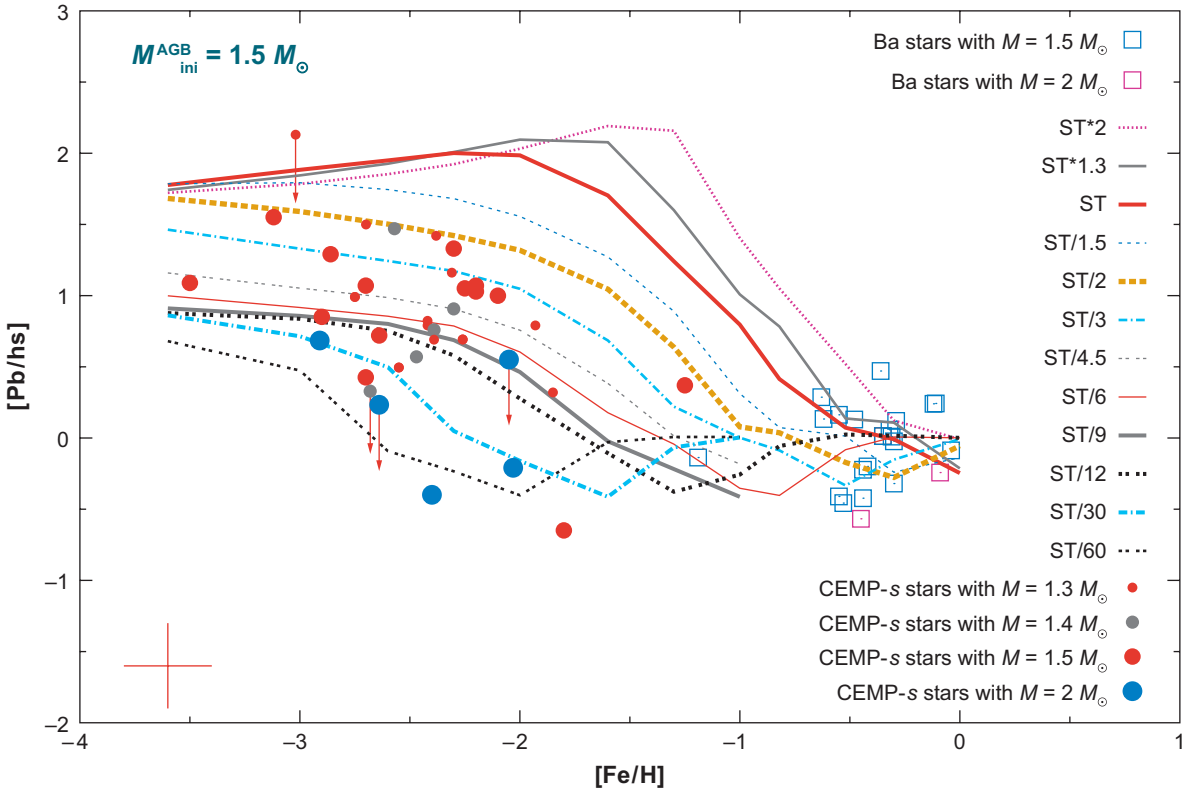

Figure 20

Theoretical [Pb/hs] versus [Fe/H] relations as predicted by AGB models of initial mass 1.5 $M_\odot$ and different ^{13}C-pocket efficiencies as indicated in the labels. The predictions are compared with representative points of CEMP-*s* and Galactic Ba stars with reported Pb abundances (Allen & Barbuy 2006). The data points for the CEMP stars and the criteria adopted for the inferred AGB mass of each star are the same as in **Figure 19**.

with the envelope at any TDU episode does not contain any ^{14}N, which was fully converted to ^{22}Ne in the previous thermal pulse. Also ^{13}C is not present in TDU matter. This implies that in the envelope very large ^{12}C/^{13}C ratios would be expected.

A large amount of ^{22}Ne is present in a thermal pulse. The H-burning shell converts CNO nuclei into ^{14}N. This is followed by the α chain ^{14}N(α, γ) ^{18}F($\beta^+\nu$)^{18}O(α, γ) ^{22}Ne occurring in the early phases of the thermal instability. Production of ^{22}Ne also comes from the primary ^{12}C mixed with the envelope by previous TDU episodes, converted to primary ^{14}N by H shell burning and then to ^{22}Ne in the next thermal pulse. The impact of this primary source becomes predominant in very metal-poor AGB stars and has been discussed in Gallino et al. (2006). In particular, enhanced ^{23}Na is produced in the thermal pulse by *n*-capture on the abundant ^{22}Ne (in spite of its small capture cross-section, Bao et al. 2000). After the last TDU it is predicted that [Na/Fe] ∼ [Ne/Fe] (with Ne almost pure ^{22}Ne) in the AGB envelope. A large ^{22}Ne content can also lead to a huge enhancement of [Mg/Fe] arising from the ^{22}Ne(α, n) ^{25}Mg and ^{22}Ne(α, γ) ^{26}Mg reactions. Thus, in CEMP-*s* stars the Mg isotopic ratios are expected to be extremely anomalous with respect to the Solar isotopic composition.

AGB models of lower initial mass (e.g., 1.3–1.4 $M_\odot$) suffer fewer (4–10) thermal pulses followed by TDU. The resulting nucleosynthesis characteristics are lower C, Na (and Mg), and

s-process abundances. Lower-mass AGB models (<1.5 $M_\odot$) also produce higher [hs/ls] values than do higher-mass stars that undergo more thermal pulses. To illuminate these ideas, consider the CEMP-*s* dwarf star CS 22898-027 ([Fe/H] ≈ -2.3) (Preston & Sneden 2001; Aoki et al. 2002c, 2007a). In **Figure 21*a*** this abundance set is compared with an AGB model of the same metallicity, initial mass 2 $M_\odot$ and ^{13}C pocket case ST/9. The raw AGB star has predicted hs elements and Pb about 1.15 dex higher than are observed (*upper dashed curve*). Once a dilution factor dil = 1.15 dex is applied, the hs elements and Pb are satisfactorily reproduced, but [Eu/Fe] turns out to be 0.75 dex lower than observed. For this star, [La/Eu] = 0.25, indicative of a CEMP-*s* star with a huge *r*-process overabundance in addition to the *s*-process enhancements. To repair this deficiency, an *r*-process excess is assumed in the original CS 22898-027 material ($[r/Fe]^{ini} = +2$) prior to acquisition of *s*-process material from the AGB companion. Applying that adjustment and dil = 1.15 dex, the resulting predicted element distribution is satisfactory for the hs and Pb elements. For this case Dy and Er, which belong to the same *r*-process peak as Eu, are also better reproduced.

Although the abundance comparison is generally good, some striking anomalies remain for CS 22898-027. The ls elements Y and Zr are clearly overpredicted by ~0.5 dex with respect to the observed abundances, and the predicted Na is higher by ~0.8 dex. These anomalies can be cured by assuming an AGB model of initial mass 1.3 $M_\odot$, no dilution, $[r/Fe]^{ini} = 2$ and ^{13}C pocket case ST/12, as is shown in **Figure 21*b***. As discussed above, a lower [C/Fe] value in the envelope might result from the CBP activation during the AGB phase. A reduction of 0.4 dex in [C/Fe] would increase the predicted [N/Fe] ratio by about 1 dex. The remaining anomaly is the observed very low [Al/Fe] value. None of the AGB models can match this abundance.

There is a high fraction of binary CEMP-*s*+*r* stars. One possible explanation has been offered by Cameron, Vanhala & Höflich (1997) and Vanhala & Cameron (1998). They showed through numerical simulations how the supernova ejecta at high velocities may interact with a nearby molecular cloud, inducing Rayleigh-Taylor instabilities in the cloud and polluting it with fresh nucleosynthesized material, and at the same time triggering the condensation of a binary system of low mass. Other explanations for these peculiar CEMP-*s* + *r* stars involve a combination of highly *s*-process-enriched material from an AGB companion and *r*-process-enriched material from the ejecta of an exploding massive object (e.g., Cohen et al. 2003). On the other hand, similar to CS 22880-074 (Aoki et al. 2007a), 13 other CEMP-*s* stars do not show any *r*-process-enhancement, including HE 0024-2523 (Lucatello et al. 2003), HE 2158-0348 (Cohen et al. 2006), and HE 0202-2203 (Barklem et al. 2005).

Finally, we recall recent studies of AGB stars of near-zero metallicity. The first studies (Fujimoto, Iben & Hollowell 1990; Hollowell, Iben & Fujimoto 1990; Chieffi et al. 2001; Goriely & Siess 2001) showed that for [Fe/H] = 0 and up to [Fe/H] ~ −3 the behavior of the first thermal pulse is qualitatively different to more metal-rich compositions. The initial CNO content is so low that the H-burning shell is very inefficient. The first fully developed thermal instability in the He shell may induce the convective pulse to propagate beyond the quite inefficient H-burning shell into the H-rich envelope, ingesting a large amount of hydrogen atoms in the deep convective zones where partial 3α reactions take place, producing a great amount of ^{13}C and ^{14}N. Once freshly nucleosynthesized CN is mixed with the surface layers, the subsequent H-burning shell and TDU episodes mimic the evolution of higher metallicity AGB models. Details of the thermal pulse and associated nucleosynthesis of light and *n*-capture elements during the TDU episodes for these very low-metallicity stars have been described by, e.g., Iwamoto et al. (2004); Suda et al. (2004); Suda, Fujimoto & Itoh (2007); Cristallo et al. (2006); Campbell (2007); and Campbell & Lattanzio (2008). These are very complex phenomena that need further investigation.

We emphasize that though the model calculations are quite complex and subject to a number of free as well as model-dependent parameters, they have been successful in reproducing the

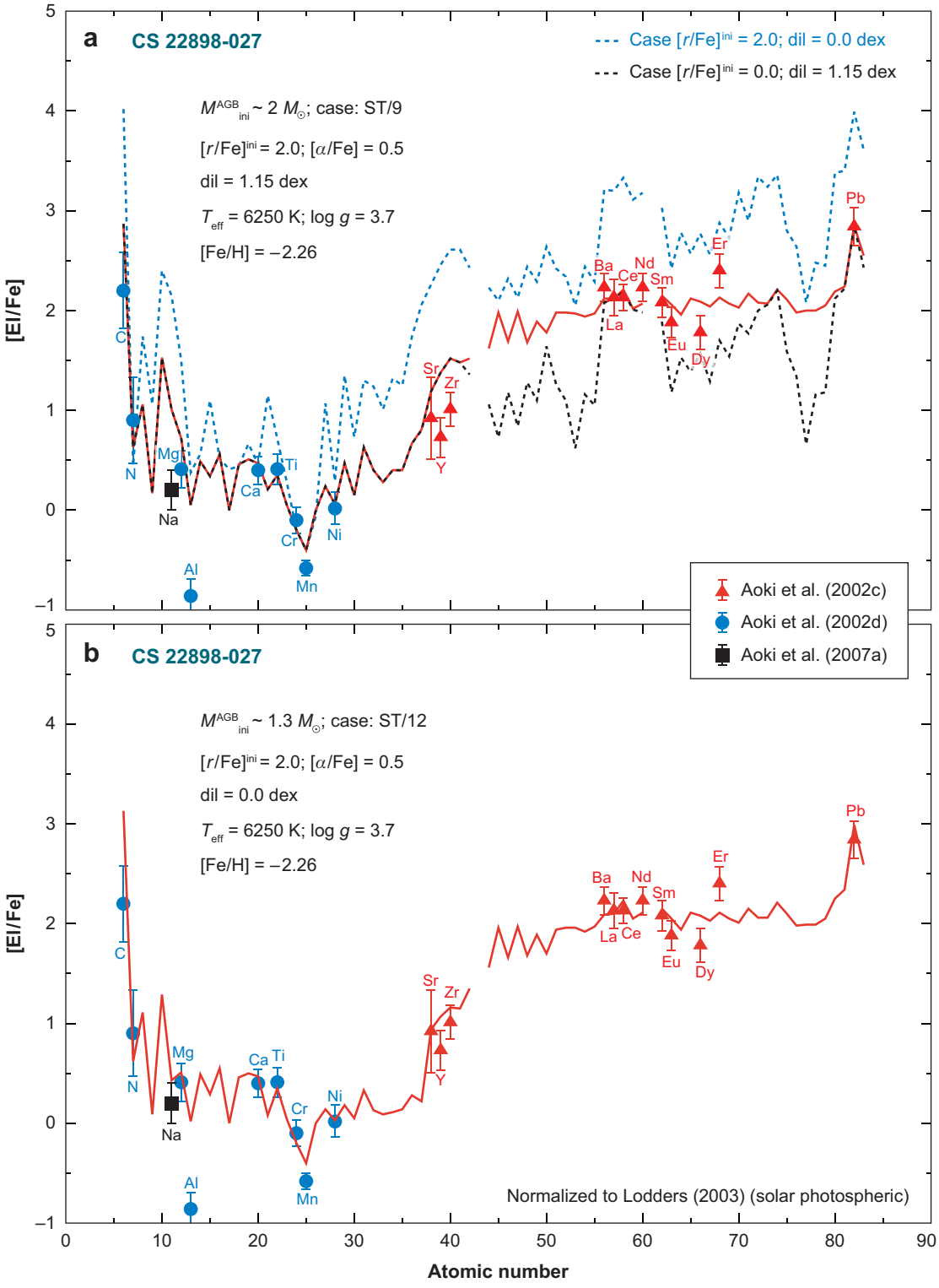

Figure 21

The observed abundances of the CEMP-$s + r$ dwarf star CS 22898-027 (Preston & Sneden 2001; Aoki et al. 2002c, 2007a) compared with predicted AGB s-process abundances diluted to match the observations. The abundances are normalized to Solar photospheric abundances of Lodders (2003). (*a*) The AGB model has [Fe/H] −2.3, initial mass 2 $M_{\odot}$ and ^{13}C pocket case ST/9. The blue dashed curve assumes no dilution and no underlying r-process enhancements. The black dashed curve shows the application of a dilution factor dil = 1.15 dex. The red solid curve keeps that dilution but adds in an assumed $[r/Fe]^{ini} = 2$. The red curve matches the hs elements and Pb well, but overpredicts the ls elements, as well as Na and Al. (*b*) The best match between predicted and observed CS 22898-027 abundances. The major change is the lower AGB mass, done to improve the match for the $Z \leq 30$ elements. This in turn yields a lower dilution factor, dil = 0.

abundance patterns seen in the metal-poor, CEMP stars. However the theoretical models we envisaged are quite possibly far from the reality. All in all, in this fascinating field we have to be guided by observations.

9. SUMMARY AND CONCLUSIONS

We have reviewed the formation of the rare, but important, neutron-capture elements in the early Galaxy. These elements are produced by stars in either the s- or the r-process. In the case of the r-process, formation in explosive environments (i.e., supernovae) is suspected but not confirmed. Observational and theoretical studies have confirmed that AGB stars are the sites for s-process synthesis. Solar-system abundances are, in fact, an amalgamation of the two processes. Much progress in deconvolving the contributions of each synthesis mechanism has resulted from more precise Solar-system abundance determinations and from increasingly accurate nuclear physics data on the neutron-rich isotopes.

Observations of the n-capture elements in old, low-mass Galactic halo stars are providing new insights into the nature of the earliest generations of stars. This includes the first stars, which have long since disappeared and were the progenitors of the halo stars. In addition the observations provide clues about the nature and types of early synthesis mechanisms for the elements, particularly at very low metallicities.

SUMMARY POINTS

1. Among very low-metallicity (and presumably very old) Galactic stars, many show predominantly r-process abundance patterns. This suggests that the sites for the r-process were short-lived, rapidly evolving, and probably high-mass, synthesizing the elements and ejecting them into space prior to the formation of the halo stars. The bulk of Galactic s-process nucleosynthesis occurred much later owing to the long evolution timescales of the lower mass stars that are the sites for this synthesis process.
2. A number of C- and s-process-rich stars, however, do exist at low metallicities in the early Galaxy. Radial velocity studies suggest that these stars result from binary-star mass transfer from more massive companions that become compact objects.
3. The abundance patterns of the heavy stable elements from Ba through Pb in the most metal-poor, but neutron-capture-rich stars are consistent with the scaled or relative Solar-system r-process-only element abundance pattern. The agreement has become progressively better for more and more elements as a result of increasingly precise experimental

atomic physics data on transition probabilities and on hyperfine and isotopic substructure. These results in turn suggest a robust *r*-process, at least for the heavier elements, over the lifetime of the Galaxy. Isotopic abundance fractions of Ba, Nd, Sm, and Eu are consistent with the element abundance patterns.

4. In contrast to the heavier elements, the lighter *n*-capture elements do not appear to be consistent with the Solar-system *r*-process abundance pattern. This may indicate that multiple *r*-process sites exist with different frequencies or stellar mass ranges for the sites associated with the lighter and heavier *n*-capture elements. Also, non-neutron-capture processes (primary in nature) may contribute to the lighter elements.
5. Abundance comparisons of halo and disk stars as a function of metallicity indicate scatter for *r*-process elements, represented by Eu, at very low metallicity, suggesting that *r*-process production was rare early in the Galaxy. This behavior is not seen in the α-element Mg, possibly indicating different sites, and/or mass ranges, for the synthesis of these two types of elements.
6. Further evidence of differences between *r*- and *s*-process production is indicated by the ratio of the *s*-process element La to Eu as a function of metallicity. At the very lowest metallicities, the ratios for many stars are consistent with the *r*-process-only value, but indications of some *s*-processing occur already at only slightly higher metallicities.
7. The long-lived radioactive *r*-process elements such as Th and U can be employed to determine the chronometric ages of the oldest stars. This in turn places limits on the age of the Galaxy and the Universe. The chronometric results are generally in agreement with other age estimates such as globular cluster ages and cosmological age estimates.
8. The details of the *s*-process are quite complex in AGB stars and depend upon a number of parameters, including particularly the amount of the ^{13}C neutron source.
9. Detailed *s*-process models have been successful in explaining the stellar observations, including the CEMP stars at low metallicities.

FUTURE ISSUES

Improvements in our understanding of the early evolution of the Galaxy require additional observations, experiments, and theoretical advances that include, but are not limited to, the following:

1. Large-scale observational surveys are needed to search for increasingly metal-poor stars. Such studies may help to identify the nature of the first stars as well as to discover additional *r*-process-rich, ultrametal-poor stars. Detailed individual stellar analyses will require increasingly high spectral resolution and broad spectral coverage to obtain more elemental and isotopic abundance patterns in the most metal-poor stars.
2. We also need additional experimental atomic data, including transition probabilities and hyperfine/isotopic patterns. These atomic data will lead to increasingly precise stellar abundance estimates. Complementary nuclear physics studies, both experimental and theoretical advances in determining the properties for neutron-rich nuclei, will also be necessary to understand the nature of neutron synthesis mechanisms.

3. Stellar evolution studies, particularly to understand the explosion mechanism and the associated physics for supernovae, are required to make headway on the physics of the *r*-process. Although the site for the *s*-process is confirmed, future work is necessary to identify the astrophysical site for the *r*-process.

DISCLOSURE STATEMENT

The authors are not aware of any biases that might be perceived as affecting the objectivity of this review.

ACKNOWLEDGMENTS

We thank all of our colleagues for their helpful advice and particularly Sara Bisterzo and Laura Husti for the Figures in Section 8, and Ian Roederer for comments on the manuscript. We also thank J. Collier for help with the abundance tables and analyses. This work has been supported in part by the National Science Foundation through grants AST-0607708 to C.S. and AST-0707447 to J.J.C., and from the Italian MIUR-PRIN06 Project "Late phases of Stellar Evolution: Nucleosynthesis in Supernovae, AGB stars, Planetary Nebulae."

LITERATURE CITED

Abia C, Domínguez I, Gallino R, Busso M, Masera S, et al. 2002. *Ap. J.* 579:817
Allen DM, Barbuy B. 2006. *Astron. Astrophys.* 454:895
Anders E, Grevesse N. 1989. *Geochim. Cosmochim. Acta* 53:197
Aoki W, Ando H, Honda S, Iye M, Izumiura H, et al. 2002a. *Publ. Astron. Soc. Jpn.* 54:427
Aoki W, Beers TC, Christlieb N, Norris JE, Ryan SG, Tsangarides S. 2007a. *Ap. J.* 655:492
Aoki W, Bisterzo S, Gallino R, Beers T, Norris JE, Ryan SG. 2006a. *Ap. J.* 650:127
Aoki W, Frebel A, Christlieb N, Norris JE, Beers TC, et al. 2006b. *Ap. J.* 639:897
Aoki W, Honda S, Beers TC, Kajino T, Ando H, et al. 2005. *Ap. J.* 632:611
Aoki W, Honda S, Beers TC, Sneden C. 2003a. *Ap. J.* 586:506
Aoki W, Honda S, Beers TC, Takada-Hidai M, Iwamoto N, et al. 2007b. *Ap. J.* 660:747
Aoki W, Honda S, Sadakane K, Arimoto N. 2007c. *Publ. Astron. Soc. Jpn.* 59:519
Aoki W, Norris JE, Ryan SG, Beers TC, Ando H. 2002b. *Ap. J.* 567:1166
Aoki W, Ryan SG, Iwamoto N, Beers TC, Norris JE, et al. 2003b. *Ap. J.* 592:L67
Aoki W, Ryan SG, Norris JE, Beers TC, Ando H, Tsangarides S. 2002c. *Ap. J.* 580:1149
Argast D, Samland M, Thielemann F-K, Qian Y-Z. 2004. *Astron. Astrophys.* 416:997
Arlandini C, Käppeler F, Wisshak K, Gallino R, Lugaro M, et al. 1999. *Ap. J.* 525:886
Arnone E, Ryan SG, Argast D, Norris JE, Beers TC. 2005. *Astron. Astrophys.* 430:507
Arnould M, Goriely S. 2003. *Phys. Rep.* 384:1
Arnould M, Goriely S, Takahashi K. 2008. *Phys. Rep.* 450:97
Bao ZY, Beer H, Käppeler F, Voss F, Wisshak K, Rauscher T. 2000. *Atomic Data Nucl. Data Tables* 76:70
Barbuy B, Spite M, Spite F, Hill V, Cayrel R, et al. 2005. *Astron. Astrophys.* 429:1031
Barklem PS, Christlieb N, Beers TC, Hill V, Bessell MS, et al. 2005. *Astron. Astrophys.* 439:129
Beers TC, Christlieb N. 2005. *Annu. Rev. Astron. Astrophys.* 43:531
Beers TC, Preston GW, Shectman SA. 1992. *Astron. J.* 103:1987
Biémont E, Quinet P. 2003. *Phys. Scr.* T105:38
Bisterzo S, Gallino R, Straniero O, Ivans II, Käppeler F, Aoki W. 2006a. *Mem. Soc. Astron. Ital.* 77:985
Bisterzo S, Käppeler F, Gallino R, Heil M, Domingo-Pardo C. 2006b. In *Int. Symp. Nucl. Astrophys.—Nuclei in the Cosmos IX, Geneva, Proc. Sci.*, PoS 77

Bromm V, Larson RB. 2004. *Annu. Rev. Astron. Astrophys.* 42:79
Burbidge EM, Burbidge GR, Fowler WA, Hoyle F. 1957. *Rev. Mod. Phys.* 29:547
Burris DL, Pilachowski CA, Armandroff TA, Sneden C, Cowan JJ, Roe H. 2000. *Ap. J.* 544:302
Busso M, Gallino R, Lambert DL, Travaglio C, Smith V. 2001. *Ap. J.* 557:802
Busso M, Gallino R, Wasserburg GJ. 1999. *Annu. Rev. Astron. Astrophys.* 37:239
Busso M, Straniero O, Gallino R, Abia C. 2004. In *Carnegie Observatories Astrophysics Ser.* Vol. 4: *Origin and Evolution of the Elements*, ed. A McWilliam, M Rauch, p. 67. Cambridge, UK: Cambridge Univ. Press
Butcher HR. 1987. *Nature* 328:127
Cameron AGW. 1957a. *Publ. Astron. Soc. Pac.* 69:201
Cameron AGW. 1957b. *Astron. J.* 62:9
Cameron AGW. 1959. *Ap. J.* 129:676
Cameron AGW. 1973. *Space Sci. Rev.* 15:121
Cameron AGW. 2001. *Ap. J.* 562:456
Cameron AGW. 2003. *Ap. J.* 587:327–40
Cameron AGW, Vanhala HAT, Höflich P. 1997. In *Proc. AIP Conf. 402*, *Astrophysical Implications of the Laboratory Study of PreSolar Materials*, ed. TJ Bernatowicz, E Zinner, p. 667. Woodbury, NY: Am. Inst. Phys.
Campbell SW. 2007. PhD thesis. Monash Univ., Aust.
Campbell SW, Lattanzio JC. 2008. In *Proc. AIP Conf. 990*, *First Stars III*, ed. BW O'Shea, A Heger, T Abel, p. 315. Woodbury, NY: Am. Inst. Phys.
Cassisi S, Castellani M, Caputo F, Castellani V. 2004. *Astron. Astrophys.* 426:641
Cayrel R, Depagne E, Spite M, Hill V, Spite F, et al. 2004. *Astron. Astrophys.* 416:1117
Cayrel R, Hill V, Beers TC, Barbuy B, Spite M, et al. 2001. *Nature* 409:691
Chieffi A, Domínguez I, Limongi M, Straniero O. 2001. *Ap. J.* 554:1159
Christlieb N, Beers TC, Barklem PS, Bessell MS, Hill V, et al. 2004. *Astron. Astrophys.* 428:1027
Christlieb N, Bessell MS, Beers TC, Gustafsson B, Korn A, et al. 2002. *Nature* 419:904
Clayton DD. 1968. *Principles of Stellar Evolution and Nucleosynthesis*. New York: McGraw-Hill
Clayton DD, Fowler WA, Hull T, Zimmerman BA. 1961. *Ann. Phys.* 12:331
Clayton DD, Rassbach ME. 1967. *Ap. J.* 148:69
Cohen JG, Christlieb N, McWilliam A, Shectman SA, Thompson I, et al. 2004. *Ap. J.* 612:1107
Cohen JG, Christlieb N, Qian Y-Z, Wasserburg GJ. 2003. *Ap. J.* 588:1082
Cohen JG, McWilliam A, Shectman S, Thompson I, Christlieb N, et al. 2006. *Astron. J.* 132:137
Cohen JG, Shectman S, Thompson I, McWilliam A, Christlieb N, et al. 2005. *Ap. J.* 633:L109
Cowan JJ, Lawler JE, Sneden C, Den Hartog EA, Collier J. 2006. In *Proc. NASA LAW 2006*, p. 82. Moffett Field, CA: NASA Ames
Cowan JJ, McWilliam A, Sneden C, Burris DL. 1997. *Ap. J.* 480:246
Cowan JJ, Pfeiffer B, Kratz K-L, Thielemann F-K, Sneden C, et al. 1999. *Ap. J.* 521:194
Cowan JJ, Sneden C. 2004. In *Carnegie Observatories Astrophysics Ser.*, Vol. 4: *Origin and Evolution of the Elements*, ed. A McWilliam, M Rauch, p. 27. Cambridge: Cambridge Univ. Press
Cowan JJ, Sneden C. 2006. *Nature* 440:1151
Cowan JJ, Sneden C, Beers TC, Lawler JE, Simmerer J, et al. 2005. *Ap. J.* 627:238
Cowan JJ, Sneden C, Burles S, Ivans II, Beers TC, et al. 2002. *Astrophys. J.* 572:861
Cowan JJ, Thielemann F-K. 2004. *Phys. Today* 57:47
Cowan JJ, Thielemann F-K, Truran JW. 1991a. *Phys. Rep.* 208:267
Cowan JJ, Thielemann F-K, Truran JW. 1991b. *Annu. Rev. Astron. Astrophys.* 29:447
Cristallo S, Straniero O, Gallino R, Piersanti L, Domínguez I. 2006. In *Int. Symp. Nucl. Astrophys.—Nuclei in the Cosmos* IX, Geneva. *Proc. Sci.*, PoS 62
Dauphas N. 2005. *Nature* 435:1203
de Laverny P, Abia C, Domínguez I, Plez B, Straniero O, et al. 2006. *Astron. Astrophys.* 446:1107
del Peloso EF, da Silva L, Porto de Mello GF, Arany-Prado LI. 2005. *Astron. Astrophys.* 440:1153
Demarque P, Woo J-H, Kim Y-C, Yi SK. 2004. *Ap. J. Suppl.* 155:667
Den Hartog EA, Herd MT, Lawler JE, Sneden C, Cowan JJ, Beers TC. 2005. *Ap. J.* 619:639
Den Hartog EA, Lawler JE, Sneden C, Cowan JJ. 2003. *Ap. J. Suppl.* 148:543

Den Hartog EA, Lawler JE, Sneden C, Cowan JJ. 2006. *Ap. J. Suppl.* 167:292
Depagne E, Hill V, Spite M, Spite F, Plez B, et al. 2002. *Astron. Astrophys.* 390:187
Dillmann I, Kratz K-L, Wöhr A, Arndt O, Brown BA, et al. 2003. *Phys. Rev. Lett.* 91:162503
Fields BD, Truran JW, Cowan JJ. 2002. *Ap. J.* 575:845
François P, Depagne E, Hill V, Spite M, Spite F, et al. 2007. *Astron. Astrophys.* 476:935
François P, Spite M, Spite F. 1993. *Astron. Astrophys.* 274:821
Frebel A, Aoki W, Christlieb N, Ando H, Asplund M, et al. 2005. *Nature* 434:871
Frebel A, Christlieb N, Norris JE, Thom C, Beers TC, Rhee J. 2007. *Ap. J.* 660:L117
Freeman K, Bland-Hawthorn J. 2002. *Annu. Rev. Astron. Astrophys.* 40:487
Freiburghaus C, Rosswog S, Thielemann F-K. 1999. *Ap. J.* 525:L121
Fröhlich C, Martinez-Pinedo G, Liebendörfer M, Thielemann F-K, Bravo E, et al. 2006. *Phys. Rev. Lett.* 96:142502
Fujimoto MY, Iben I Jr, Hollowell D. 1990. *Ap. J.* 349:580
Fulbright JP. 2000. *Astron. J.* 120:1841
Gallino R, Arlandini C, Busso M, Lugaro M, Travaglio C, et al. 1998. *Ap. J.* 497:388
Gallino R, Bisterzo S, Husti L, Käppeler F, Cristallo S, Straniero O. 2006. In *Int. Symp. Nucl. Astrophys.—Nuclei in the Cosmos IX*, Geneva. *Proc. Sci.*, PoS 100
Gallino R, Wasserburg GJ, Busso M, Straniero O. 2005. In *From Lithium to Uranium: Elemental Tracers of Early Cosmic Evolution*, ed. V Hill, P François, F Primas, Proc. IAU Symp. 228, p. 461. Cambridge, UK: Cambridge Univ. Press
Geisler D, Wallerstein G, Smith VV, Casetti-Dinescu DI. 2007. *Publ. Astron. Soc. Jpn.* 119:939
Gilroy KK, Sneden C, Pilachowski CA, Cowan JJ. 1988. *Ap. J.* 327:298
Goriely S, Arnould M. 2001. *Astron. Astrophys.* 379:1113
Goriely S, Mowlavi N. 2000. *Astron. Astrophys.* 362:599
Goriely S, Siess L. 2001. *Astron. Astrophys.* 378:25
Goswami A, Aoki W, Beers TC, Christlieb N, Norris JE, et al. 2006. *MNRAS* 372:343
Gratton R, Sneden C, Carretta E. 2004. *Annu. Rev. Astron. Astrophys.* 42:385
Grevesse N, Asplund M, Sauval AJ. 2007. *Space Sci. Rev.* 130:105
Grevesse N, Sauval AJ. 1998. *Space Sci. Rev.* 85:161
Griffin R, Gustafsson B, Vieira T, Griffin R. 1982. *MNRAS* 198:637
Hansen BMS, Richer HB, Fahlman GG, Stetson PB, Brewer J, et al. 2004. *Ap. J. Suppl.* 155:551
Hauge Ø. 1972. *Sol. Phys.* 27:286
Helfer HL, Wallerstein G, Greenstein JL. 1959. *Ap. J.* 129:700
Herwig F. 2005. *Annu. Rev. Astron. Astrophys.* 43:435
Hill V, Plez B, Cayrel R, Beers TC, Nordström B, et al. 2002. *Astron. Astrophys.* 387:560
Hillebrandt W. 1978. *Space Sci. Rev.* 21:639
Hollowell D, Iben I Jr. 1988. *Ap. J.* 333:L25
Hollowell D, Iben I Jr, Fujimoto MY. 1990. *Ap. J.* 351:245
Honda S, Aoki W, Ishimaru Y, Wanajo S, Ryan SG. 2006. *Ap. J.* 643:1180
Honda S, Aoki W, Kajino T, Ando H, Beers TC, et al. 2004. *Ap. J.* 607:474
Ishimaru Y, Wanajo S. 1999. *Ap. J.* 511:L33
Ivans II, Simmerer J, Sneden C, Lawler JE, Cowan JJ, et al. 2006. *Ap. J.* 645:613
Ivans II, Sneden C, Gallino R, Cowan JJ, Preston GW. 2005. *Ap. J.* 627:L165
Ivans II, Sneden C, James CR, Preston GW, Fulbright JP, et al. 2003. *Ap. J.* 592:906
Iwamoto N, Kajino T, Mathews GJ, Fujimoto MY, Aoki W. 2004. *Ap. J.* 602:377
Jimenez R, Verde L, Treu T, Stern S. 2003. *Ap. J.* 593:622
Johnson JA. 2002. *Ap. J. Suppl.* 139:219
Johnson JA, Bolte M. 2001. *Ap. J.* 554:888
Johnson JA, Bolte M. 2002a. *Ap. J.* 579:87
Johnson JA, Bolte M. 2002b. *Ap. J.* 579:616
Johnson JA, Bolte M. 2004. *Ap. J.* 605:462
Jonsell K, Barklem PS, Gustafsson B, Christlieb N, Hill V, et al. 2006. *Astron. Astrophys.* 451:651
Käppeler F, Beer H, Wisshak K. 1989. *Rep. Prog. Phys.* 52:945

Käppeler F, Beer H, Wisshak K, Clayton DD, Macklin RL, Ward RA. 1982. *Ap. J.* 257:821
Käppeler F, Gallino R, Busso M, Picchio G, Raiteri CM. 1990. *Ap. J.* 354:630
Kratz K-L, Faroqui K, Pfeiffer B, Truran JW, Sneden C, Cowan JJ. 2007. *Ap. J.* 662:39
Kratz K-L, Pfeiffer B, Cowan JJ, Sneden C. 2004. *New Astron. Rev.* 48:105
Krauss LM, Chaboyer B. 2003. *Science* 299:65
Lambert DL. 1992. *Astron. Astrophys.* 3:201
Lambert DL, Allende Prieto C. 2002. *MNRAS* 335:325
Lattimer JM, Mackie F, Ravenhall DG, Schramm DN. 1977. *Ap. J.* 213:225
Lawler JE, Den Hartog EA, Labby ZE, Sneden C, Cowan JJ, Ivans II. 2007. *Ap. J. Suppl.* 169:120
Lawler JE, Den Hartog EA, Sneden C, Cowan JJ. 2006. *Ap. J. Suppl.* 162:227
Lawler JE, Sneden C, Cowan JJ. 2004. *Ap. J.* 604:850
Lawler JE, Wickliffe ME, Den Hartog EA, Sneden C. 2001. *Ap. J.* 563:1075
LeBlanc JM, Wilson JR. 1970. *Ap. J.* 161:541
Lodders K. 2003. *Ap. J.* 591:1220
Lucatello S, Beers TC, Christlieb N, Barklem PS, Rossi S, et al. 2006. *Ap. J.* 652:L37
Lucatello S, Gratton R, Cohen JG, Beers TC, Christlieb N, et al. 2003. *Astron. J.* 125:875
Lucatello S, Tsangarides S, Beers TC, Carretta E, Gratton RG, Ryan SG. 2005. *Ap. J.* 625:825
Lundqvist M, Nilsson H, Wahlgren GM, Lundberg H, Xu HL, et al. 2006. *Astron. Astrophys.* 450:407
Lundqvist M, Wahlgren GM, Hill V. 2007. *Astron. Astrophys.* 463:693
Lunney D, Pearson JM, Thibault C. 2003. *Rev. Mod. Phys.* 75:1021
Magain P. 1995. *Astron. Astrophys.* 297:686
Malcheva G, Blagoev K, Mayo R, Ortiz M, Xu HL, et al. 2006. *MNRAS* 367:754
Mashonkina L, Zhao G. 2006. *Astron. Astrophys.* 456:313
Mathews GJ, Bazan G, Cowan JJ. 1992. *Ap. J.* 391:719
Mathews GJ, Cowan JJ. 1990. *Nature* 345:491
McClure RD. 1984. *Ap. J.* 280:L31
McClure RD. 1997. *Publ. Astron. Soc. Pac.* 109:536
McClure RD, Fletcher JM, Nemec JM. 1980. *Ap. J.* 238:L35
McClure RD, Woodsworth AW. 1990. *Ap. J.* 352:709
McWilliam A. 1997. *Annu. Rev. Astron. Astrophys.* 35:503
McWilliam A, Preston GW, Sneden C, Searle L. 1995. *Astron. J.* 109:2757
Merrill PW. 1952. *Ap. J.* 116:21
Meyer BS. 1994. *Annu. Rev. Astron. Astrophys.* 32:153
Mishenina TV, Kovtyukh VV. 2001. *Astron. Astrophys.* 370:951
Möller P, Nix JR, Kratz K-L. 1997. *Atomic Data Nucl. Data Tables* 66:131
Montes F, Beers TC, Cowan J, Elliot T, Farouqi K, et al. 2007. *Ap. J.* 671:1685
Moore CE, Minnaert MGJ, Houtgast J. 1966. *The Solar Spectrum 2934 Å to 8770 Å. NBS Monogr. 61.* Washington, DC: U.S. GPO
Ning H, Qian Y-Z, Meyer BS. 2007. *Ap. J.* 667:L159
Nollett KM, Busso M, Wasserburg GJ. 2003. *Ap. J.* 582:1036
Norris JE, Christlieb N, Korn AJ, Eriksson K, Bessell MS, et al. 2007. *Ap. J.* 670:774
O'Brien S, Dababneh S, Heil M, Käppeler F, Plag R, et al. 2003. *Phys. Rev. C* 68:035801
Otsuki K, Honda S, Aoki W, Kajino T, Mathews GJ. 2006. *Ap. J.* 641:L117
Pagel BEJ. 1965. *R. Greenwich Obs. Bull.* 104:127
Payne CH. 1925. PhD thesis. Radcliffe College
Peterson RC. 1976. *Ap. J.* 206:800
Pfeiffer B, Kratz K-L, Thielemann F-K. 1997. *Z. Phys. A* 357:235
Plez B, Hill V, Cayrel R, Spite M, Barbuy B, et al. 2004. *Astron. Astrophys.* 428:9
Preston GW, Beers TC, Shectman SA. 1994. *Astron. J.* 108:538
Preston GW, Sneden C. 2000. *Astron. J.* 120:1014
Preston GW, Sneden C. 2001. *Astron. J.* 122:1545
Preston GW, Thompson IB, Sneden C, Stachowski G, Shectman SA. 2006. *Astron. J.* 132:1714
Qian Y-Z, Sargent WLW, Wasserburg G. 2002. *Ap. J.* 569:L61

Qian Y-Z, Wasserburg GJ. 2000. *Phys. Rep.* 333:77
Qian Y-Z, Wasserburg GJ. 2001. *Ap. J.* 559:925
Qian Y-Z, Wasserburg GJ. 2002. *Ap. J.* 567:515
Qian Y-Z, Wasserburg GJ. 2003. *Ap. J.* 588:1099
Qian Y-Z, Wasserburg GJ. 2007. *Phys. Rep.* 442:237
Raiteri CM, Villata M, Gallino R, Busso M, Cravanzola A. 1999. *Ap. J.* 518:L91
Reddy BE, Lambert DL, Allende Prieto C. 2006. *MNRAS* 367:1329
Reddy BE, Tomkin J, Lambert DL, Allende Prieto C. 2003. *MNRAS* 340:304
Roederer IU, Lawler JE, Sneden C, Cowan JJ, Sobeck JS, Pilachowski CA. 2008. *Ap. J.* 675:723
Rossi S, Beers TC, Sneden C, Sevastyanenko T, Rhee J, Marsteller B. 2005. *Astron. J.* 130:2804
Rosswog S, Liebendörfer M, Thielemann F-K, Davies MB, Benz W, Piran T. 1999. *Astron. Astrophys.* 341:499
Russell HN. 1929. *Ap. J.* 70:11
Ryan SG, Norris JE, Beers TC. 1996. *Ap. J.* 471:254
Schatz H, Toenjes R, Kratz K-L, Pfeiffer B, Beers TC, et al. 2002. *Ap. J.* 579:626
Seeger PA, Fowler WA, Clayton DD. 1965. *Ap. J. Suppl.* 11:121
Shetrone M, Venn KA, Tolstoy E, Primas F, Hill V, Kaufer A. 2003. *Astron. J.* 125:684
Simmerer J, Sneden C, Cowan JJ, Collier J, Woolf VM, Lawler JE. 2004. *Ap. J.* 617:1091
Sneden C, Cowan JJ. 2003. *Science* 299:70
Sneden C, Cowan JJ, Ivans II, Fuller GM, Burles S, et al. 2000a. *Ap. J.* 533:L139
Sneden C, Cowan JJ, Lawler JE, Burles S, Beers TC, Fuller GM. 2002. *Ap. J.* 566:L25
Sneden C, Cowan JJ, Lawler JE, Ivans II, Burles S, et al. 2003. *Ap. J.* 591:936
Sneden C, Johnson J, Kraft RP, Smith GH, Cowan JJ, Bolte MS. 2000b. *Ap. J.* 536:L85
Sneden C, Kraft RP, Shetrone MD, Smith GH, Langer GE, Prosser CF. 1997. *Astron. J.* 114:1964
Sneden C, Lawler JE. 2008. In *Proc. AIP Conf. 990*, *First Stars III*, ed. BW O'Shea, A Heger, T Abel, p. 90. Woodbury, NY: Am. Inst. Phys.
Sneden C, McWilliam A, Preston GW, Cowan JJ, Burris DL, Armosky BJ. 1996. *Ap. J.* 467:819
Sneden C, Parthasarathy M. 1983. *Ap. J.* 267:757
Sneden C, Preston GW, Cowan JJ. 2003. *Ap. J.* 592:504
Sneden C, Preston GW, McWilliam A, Searle L. 1994. *Ap. J.* 431:L27
Spergel DN, Verde L, Peiris HV, Komatsu, Nolta MR, et al. 2003. *Ap. J. Suppl.* 148:175
Spite M, Spite F. 1978. *Astron. Astrophys.* 67:23
Straniero O, Chieffi A, Limongi M, Gallino R, Busso M, Arlandini C. 1997. *Ap. J.* 478:332
Straniero O, Domínguéz I, Cristallo S, Gallino R. 2003. *Publ. Astron. Soc. Aust.* 20:389
Straniero O, Gallino R, Cristallo S. 2006. *Nucl. Phys. A* 777:311
Suda T, Aikawa M, Machida MN, Fujimoto MY, Iben I Jr. 2004. *Ap. J.* 611:476
Suda T, Fujimoto MY, Itoh N. 2007. *Ap. J.* 667:1206
Suess HE, Urey HC. 1956. *Rev. Mod. Phys.* 28:53
Takahashi K, Witti J, Janka T. 1994. *Astron. Astrophys.* 286:857
Tegmark M, Strauss MA, Blanton MR, Abazajian K, Dodelson S, et al. 2004. *Phys. Rev. D* 69:103501
Terasawa M, Sumiyoshi K, Yamada S, Suzuki H, Kajino T. 2002. *Ap. J.* 578:137
Terlizzi R, Abbondanno U, Aerts G, Álvarez H, Alvarez-Velarde F, et al. 2007. *Phys. Rev. C* 75:035807
Thielemann F-K, Freiburghaus C, Rosswog S, Nomoto K, Nakamura T, et al. 2000. *Mem. Soc. Astron. Ital.* 71:483
Thompson IB, Ivans II, Bisterzo S, Sneden C, Gallino R, et al. 2008. *Ap. J.* 677:596
Thompson TA. 2003. *Ap. J.* 585:L33
Timmes FX, Woosley SE, Weaver TA. 1995. *Ap. J. Suppl.* 98:617
Travaglio C, Galli D, Burkert A. 2001. *Ap. J.* 547:217
Travaglio C, Gallino R, Arnone R, Cowan JJ, Jordan F, Sneden C. 2004. *Ap. J.* 601:864
Truran JW. 1981. *Astron. Astrophys.* 97:391
Truran JW, Cowan JJ, Pilachowski CA, Sneden C. 2002. *Publ. Astron. Soc. Pac.* 114:1293
Turner MS. 2003. *Connecting Quarks with the Cosmos: Eleven Science Questions for the New Century*. Washington, DC: Natl. Acad. Press
VandenBerg DA, Bolte M, Stetson PB. 1996. *Annu. Rev. Astron. Astrophys.* 34:461

Van Eck S, Goriely S, Jorissen A, Plez B. 2001. *Nature* 412:793
Van Eck S, Goriely S, Jorissen A, Plez B. 2003. *Astron. Astrophys.* 404:291
Vanhala HAT, Cameron AGW. 1998. *Ap. J.* 508:291
Venn KA, Irwin M, Shetrone MD, Tout CA, Hill V, Tolstoy E. 2004. *Astron. J.* 128:1177
Wahlgren GM. 2002. *Phys. Scr.* 100:22
Wallerstein G, Greenstein JL, Parker R, Helfer HL, Aller L. 1963. *Ap. J.* 137:280
Wallerstein G, Knapp GR. 1998. *Annu. Rev. Astron. Astrophys.* 36:369
Wanajo S, Itoh N, Ishimaru Y, Nozawa S, Beers TC. 2002. *Ap. J.* 577:853
Wanajo S, Tamamura M, Itoh N, Nomoto K, Ishimaru Y, et al. 2003. *Ap. J.* 593:968
Wasserburg GJ, Busso M, Gallino R. 1996. *Ap. J.* 466:L109
Wasserburg GJ, Busso M, Gallino R. 2006. *Nucl. Phys. A* 777:5
Wasserburg GJ, Qian Y-Z. 2000. *Ap. J.* 529:L21
Westin J, Sneden C, Gustafsson B, Cowan JJ. 2000. *Ap. J.* 530:783
Wheeler JC, Cowan JJ, Hillebrandt W. 1998. *Ap. J.* 493:L101
Winckler N, Dababneh S, Heil M, Käppeler F, Gallino R, Pignatari M. 2006. *Ap. J.* 647:685
Woosley SE, Weaver TA. 1995. *Ap. J. Suppl.* 101:181
Woosley SE, Wilson JR, Mathews GJ, Hoffman RD, Meyer BS. 1994. *Ap. J.* 433:229
Yushchenko A, Gopka V, Goriely S, Musaev F, Shavrina A, et al. 2005. *Astron. Astrophys.* 430:255
Xu HL, Sun ZW, Dai ZW, Jiang ZK, Palmeri P, et al. 2006. *Astron. Astrophys.* 452:357

Annual Review of Astronomy and Astrophysics

Volume 46, 2008

Contents

Indexes

Errata

An online log of corrections to *Annual Review of Astronomy and Astrophysics* articles may be found at http://astro.annualreviews.org/errata.shtml